

KfK 2969
Juli 1980

Influence of Leakage Flow on the Behaviour of Gas Behind a Blockage in LMFBR Subassembly Geometry

Y. Fukuzawa
Institut für Reaktorentwicklung
Projekt Schneller Brüter

Kernforschungszentrum Karlsruhe

Kernforschungszentrum Karlsruhe
Institut für Reaktorentwicklung
Projekt Schneller Brüter

KfK 2969

Influence of Leakage Flow on the Behaviour of
Gas Behind a Blockage in LMFBR Subassembly Geometry

by
Y. Fukuzawa

Kernforschungszentrum Karlsruhe GmbH, Karlsruhe

Als Manuskript vervielfältigt
Für diesen Bericht behalten wir uns alle Rechte vor

Kernforschungszentrum Karlsruhe GmbH
ISSN 0303-4003

Abstract

Observations were made of the behaviour of gas behind a uniform porous 21 % corner blockage within a pin-bundle of LMFBR subassembly geometry. The main parameter of the experiment was the leakage flow rate through the blockage. The behaviour of gas is significantly influenced by the leakage flow rate. The measured size and residence time of a gas cavity formed behind the blockage are shown and the mechanisms of the gas cavity dispersion by the leakage flow discussed by using a simple model of the liquid flow distribution behind the blockage.

Zusammenfassung

Einfluß der Leckrate einer porösen Blockade auf das Verhalten von Gas hinter der Blockade in einer Bündel-Geometrie ähnlich einem Schnell-Brüter-Brennelement

Das Verhalten von Gasblasen im Totwassergebiet hinter einer porösen Blockade in einem Brennelement des schnellen natriumgekühlten Brutreaktors wurde mit einem simulierten Brennelement mit einer porösen 21%-Eckblockade in einem Wasserkreislauf untersucht.

Die Teststrecke repräsentierte die Hälfte eines Brennelements, wobei die Schnittebene entlang der vertikalen Symmetrieebene durch die Blockade verlief und durch eine Glasscheibe abgeschlossen war.

Wichtigster Parameter der Untersuchungen war der Restdurchsatz durch die Blockade, welcher kontinuierlich verändert werden konnte. Abhängig von der Größe des Restdurchsatzes wurde das Verhalten des Gases in starkem Maße durch diesen beeinflusst.

Ermittelt wurde die Größe der Gasansammlung hinter der Blockade, sowie deren Verweilzeit. Die Mechanismen der Auflösung einer Gasansammlung durch den Restdurchsatz werden an Hand eines einfachen Modells für die Strömungsverteilung der Flüssigkeit hinter der Blockade diskutiert.

Contents

Abstract

Zusammenfassung

List of tables

List of figures

1. Introduction

2. Previous work

2.1 Gas behaviour behind an impermeable blockage

2.2 Flow distribution behind a porous blockage

3. Experimental apparatus and method

4. Two-phase flow patterns

4.1 Circulating bubbles (Type 3)

4.2 Rising bubble (Type 1)

4.3 Gas cavity (Type 2)

5. Dispersion of gas cavity

5.1 Critical velocities for cavity formation

5.2 Critical leakage ratio for cavity dispersion

5.3 Mechanisms of gas cavity dispersion

6. Theoretical analysis

6.1 A flow model

6.1.1 Features of the model

6.1.1.1 Flow distribution behind an impermeable blockage

6.1.1.2 Flow distribution behind a porous blockage

6.1.2 Velocity distribution in the vortex

6.1.3 Change of vortex radius

6.2 Bubble motion due to buoyancy in the vortex

6.3 Prediction of critical leakage ratio

7. Transient conditions

7.1 Release rate of fission gas from a fuel pin

7.2 Pulsewise gas injection

8. Conclusions

Acknowledgement

Nomenclature

References

List of tables

- Table 1 Leakage ratio for the dispersion of circulating bubbles
- Table 2 Reverse velocity of bubbles near the wall

List of figures

- Fig. 1 Schematic diagrams of two-phase flow patterns in the wake behind an impermeable blockage [3]
- Fig. 2 Relation between flow pattern, gas injection rate and main flow velocity for an impermeable blockage [3]
- Fig. 3 Relation between flow pattern, gas injection rate and main flow velocity for an impermeable blockage [3]
- Fig. 4 Cross section of test section
- Fig. 5 Schematic side view of test section
- Fig. 6 Blockage geometry
- Fig. 7 Relation between gas injection rate, main flow velocity and flow pattern types for the blockage with no leakage flow
- Fig. 8 Change of circulating bubble region behind the blockage
- Fig. 9 Radial distribution of axial velocity of bubbles for various leakage ratios
- Fig. 10 Comparison of bubble velocity distributions for various leakage ratios
- Fig. 11 Dependence of rising velocity on axial position
- Fig. 12 Comparison between experimental and calculated results of rising velocity
- Fig. 13 Change of the flow pattern Type 2 to Type 1 by the increase of the leakage flow
- Fig. 14 Change of the flow pattern Type 2 to Type 1 by increasing leakage flow

- Fig. 15 Dependence of gas cavity size on leakage ratio
- Fig. 16 Dependence of the residence time of gas cavity on leakage ratio
- Fig. 17 Relation between gas injection rate, main flow velocity and flow pattern types for various leakage ratios
- Fig. 18 Dependence of critical velocities for gas cavity formation on leakage ratio
- Fig. 19 Dependence of critical leakage ratio for gas cavity dispersion on gas injection rate
- Fig. 20 Flow distribution behind an impermeable blockage [11_7]
- Fig. 21 Flow distribution behind a porous blockage
- Fig. 22 Schematic diagram of a comparison between "floating-" and "fixed-centre" models
- Fig. 23 A fixed-centre model for calculations of bubble motion in the central vortex
- Fig. 24 Bubble motion due to buoyancy in Region 2 of the central vortex (Calculation)
- Fig. 25 Comparison between measured and calculated critical velocity of the lower boundary
- Fig. 26 Comparison between measured and calculated values of critical leakage ratio for gas cavity dispersion
- Fig. 27 Maximum gas release rate from a fuel pin
- Fig. 28 Transient gas behaviour behind the blockage with leakage flow just after start of gas injection

1. Introduction

The phenomenon of gas bubble entrapment in the recirculating wake behind a blockage is considered to be one of the potential pin-to-pin failure propagation mechanisms due to fission gas release in the subassembly of a Liquid Metal Fast Breeder Reactor (LMFBR) [1]. If a coolant flow is locally blocked in the subassembly, a recirculating wake is formed behind the blockage and the temperature in the wake is enhanced.

Hence the possibility of fission gas release from fuel pins in the wake may be increased due to the high temperature. The released gas may accumulate in the wake, forming a gas cavity, finally causing dryout and further pin failure.

The phenomenon of gas accumulation in the wake behind a blockage was inferred from gas injection experiments in a full-scale 169-pin bundle with a 21 % corner planar blockage in sodium at Kernforschungszentrum Karlsruhe [2].

However, the information obtained from the experiments was not enough to fully describe the behaviour of gas in the wake, since the number and the position of bubble detectors, and hence data obtained, were restricted. For this reason, gas injection experiments in water, in a half-bundle with the same pin arrangement and blockage fraction as in sodium, were performed to observe directly the behaviour of gas in the wake [3].

The experimental results in water showed that a gas cavity was formed behind the blockage under some conditions, using glass rods simulating fuel pins.

In reality, a permeable blockage may be more probable than an impermeable blockage. In the permeable blockage case the behaviour of gas will be influenced by a leakage flow through the blockage.

The present report describes the influence of the leakage flow on the behaviour of gas behind a porous blockage. Observations were made of two-phase flow patterns and of gas cavity formation behind the blockage. A simple flow model was developed and the motion of bubbles behind the blockage discussed.

2. Previous work

2.1 Gas behaviour behind an impermeable blockage

The two-phase flow patterns behind a 21 % corner planar blockage in water were observed by a photographic method and described in [3]. The gas was injected into the liquid upstream and downstream of the blockage. The patterns were classified into the following three types.

Type 1: Bubbles rise up through the wake without forming a gas cavity,

Type 2: Bubbles circulate around a gas cavity,

Type 3: Bubbles circulate in the wake with no gas cavity formation.

A schematic diagram of these types is shown in Fig. 1. The gas cavity is defined as a stationary gas bubble with a radius larger than two times of the hydraulic radius of the subchannel (2.7 mm).

The relations between gas injection rate, main flow velocity and flow pattern types for the impermeable blockage are shown in Figs. 2 and 3, for the downstream and upstream gas injection cases, respectively. The flow pattern changes from Types 1 to 3 in turn with increasing velocity for any rate of gas injection. The gas cavity region is bounded by a "lower boundary" and an "upper boundary" of the main flow velocity at each gas injection rate.

In the lower velocity range corresponding to the flow pattern of Type 1, a gas cavity cannot remain in the wake, but rises up as a single bubble due to buoyancy. In the higher velocity range corresponding to the flow pattern of Type 3, the gas cavity is broken up by liquid flow forces on the main stream side of the wake, only small gas bubbles circulating in the wake. In the velocity range in between, corresponding to the flow pattern of Type 2, a gas cavity is present in the wake.

The gas cavity is sustained by two contrary effects: formation of the cavity due to gas accumulation and breakup of the cavity by liquid flow forces.

2.2 Flow distribution behind a porous blockage

Flow distribution behind a porous blockage has been studied experimentally and theoretically by various investigations.

Basmer et al. [4] performed blockage experiments in water and showed visually a recirculating flow behind a blockage. The liquid circulates, representing an elliptical streamline. With increasing leakage flow rate, the distance between the recirculating flow region and the blockage increases.

Blackburn et al. [5] calculated the flow distribution behind a blockage with a computer code SABRE. With increasing porosity, the recirculating flow region becomes smaller and its distance from the blockage increases.

Gregory and Lord [6] calculated stream function distributions and turbulence velocity profiles behind a blockage with a computer code WAKE. The flow distribution is more closely dependent upon the magnitude of the residual flow than on the type of porosity (homogeneous or discrete orifices). The turbulence velocity profile is influenced by the residual flow. For both cases of impermeable and uniform porous blockages, the maximum turbulence level is at the boundary of the main stream and the recirculating flow region.

Judd [7] performed blockage experiments in an air wind-tunnel and measured velocity distributions and turbulence levels behind a blockage. The effect of slight porosity is to extend the recirculating flow region slightly, to reduce the turbulence slightly, and to reduce the pressure perturbation. More porosity destroys the recirculating flow region, and reduces the turbulence and pressure perturbation significantly.

Robinson [8] carried out experiments with a blockage in water and compared it with calculations by the SABRE code. A transient eddy is observed at the boundary of the main stream and the recirculating flow region. Residual flow through the blockage with discrete permeability can lead to a change in the wake geometry.

The flow distribution behind a porous 21 % corner blockage was observed in water by the present author [9] and the following results were obtained:

- The downstream stagnation point is not significantly influenced by the leakage flow.
- The recirculating flow region and the reverse flow velocity near the wall decreases with increasing leakage rate.
- The recirculating flow region disappears at a "leakage ratio" of about 7 %.

The leakage ratio is defined as follows:

$$\phi = \frac{M_B}{M_0} \cdot \frac{A_0}{A_B} \quad (1)$$

where M_B is the mass flow rate through the blockage, M_0 is the total mass flow rate through the subassembly, A_0 is the total area of the main flow and A_B is the blockage area (including the area for leakage flow but not the area of fuel pins).

3. Experimental apparatus and method

The cross section of the test section used in the present experiment is shown in Fig. 4. The test section represented one half of the fuel subassembly of the MK 1a core of the SNR 300 prototype reactor. It was divided along the vertical plane of symmetry through the blockage. A glass wall occupied the position of this plane. Thin stainless steel rods (6.0mm diameter, 7.9mm pitch) were arranged to simulate fuel pins. The geometry of the test section and the fuel pin arrangement are the same as in the previous experiment with a 21% impermeable corner blockage [3].

An axially extended porous blockage with two chambers (inlet and outlet) was installed at the spacer grid in the corner of the test section. The ratio of the blocked area (including the area for leakage flow) to the total flow area is 0.21. The design of this blockage based upon a previous study to this problem [10]. A schematic side view of the test section is shown in Fig. 5. Water was pumped upwards through the test section and the flow rate measured before the inlet. The mean velocity of the main flow in the test section ranged from 1.2 to 5.9 m/s in the present experiment.

Argon, simulating fission gases, was injected into the flow behind the blockage from a hole drilled through the subassembly wall. The hole is of 0.5mm diameter 50mm above the blockage. The gas was supplied from a gas bottle. The flow rate controlled by valves was measured under steady state conditions by a Rotameter-type flow meter.

In the present experiment, the gas flow rate ranged from 1 to 30Ncm³/s (standard temperature and pressure). In a number of experiments, a gas plenum of volume 17cm³, simulating a fuel pin volume, was used for pulsewise gas injection. The initial gas pressure in the plenum was 10 bar, measured at room temperature.

In addition to the main flow loop the test section had an auxiliary loop to control the leakage flow through the blockage independently of the main flow.

The blockage geometry is shown in Fig. 6. The blockage is 42mm long and divided into two chambers by an impermeable plate. Through the bottom plate of the blockage, a hole with a diameter of 1.5mm was drilled in each blocked subchannel. In the top plate there are three holes with a diameter of 1mm in each subchannel.

A portion of the main flow in the test section was introduced via the lower chamber into the auxiliary loop and returned again to the upper chamber, being injected into the wake through the holes in the top plate. The flow rate through the auxiliary loop, simulating a leakage flow rate through the blockage, was controlled by a pump and a valve and measured by a Rotameter-type flow meter.

In the present experiment the leakage ratio defined by Eq. (1) ranged from 0 to 8%.

The behaviour of gas behind the blockage was directly observed and recorded on cine film. The film speed was varied between 500 and 2000 Frames/second, depending on experimental conditions.

4. Two-phase flow patterns

The relation between gas injection rate, main flow velocity and flow pattern types for the blockage with no leakage flow, obtained in the present experiments, is shown in Fig. 7. The gas was steadily injected behind the blockage. The same flow patterns as in the previous impermeable blockage experiment [3], described in Section 2-1, were also observed in the present experiments. The flow pattern changes from Types 1 to 3 in turn with increasing main flow velocity for any rate of gas injection.

The gas cavity region, bounded by the lower and the upper boundaries, is also similar as in Fig. 2 obtained in the previous experiments.

The influences of the leakage flow on the flow patterns are described in the following sections.

4.1 Circulating bubbles (Type 3)

The flow pattern Type 3 is characterized by gas bubbles circulating in the wake with no gas cavity formation. This is observed in the higher velocity range of the main flow.

The influence of the leakage ratio on the geometry of the circulating bubble region behind the blockage is shown in Fig. 8, where the top of the region was determined by the location where some of the bubbles went upwards and others downwards. As seen in the figure the leakage flow influences markedly the distance between the blockage and the lower part of the circulating bubble region, but not significantly the position of the top of the region. The area of the circulating bubble region decreases with increasing leakage ratio, resulting in the disappearance of the bubbles behind the blockage at a leakage ratio of about 7%.

The influence of the main flow velocity on the leakage ratio for the dispersion of the circulating bubbles is shown in Table 1. The leakage ratio increases very slightly with increasing velocity of the main flow.

The velocity of the bubbles in the region can be measured from cine film. The radial distribution of the axial component of the velocity is shown in Fig. 9 for various leakage ratios, where the velocity was normalized with respect to the main flow velocity. With increasing leakage flow rate, the centre of the circulation bubble region moves axially and radially. The axial position of the measurement was the middle of the circulating bubble region.

It may be seen that the circulating bubble region decreases with increasing leakage ratio, but the magnitude of the axial velocity for each radial position from the centre of the region is not significantly changed. A comparison between the radial distributions of the axial component of the bubble velocity for various leakage ratios is shown in Fig. 10.

The data were obtained from Fig. 9 and the radial position was measured, in each case, for the centre of the region, which depended on the leakage ratio. The velocity gradient of the bubbles within the circulating region is not significantly influenced by the leakage flow.

The reverse velocity of the bubbles increases in the radial direction. The reverse velocity near the wall gives a maximum value. The dependence of the maximum reverse velocity on the leakage ratio is shown in Table 2, where data are the average values obtained by more than ten measurements. The reverse velocity decreases markedly with increasing leakage ratio.

The bubble velocities may approximately represent liquid velocities in the wake. The circulating bubble region is nearly equal to the recirculating flow region of the liquid behind the blockage. From Figs. 8 to 10, the following may be said regarding the flow

distribution behind the blockage.

- With increasing leakage ratio, the downstream stagnation point of the wake moves downstream very slightly.
- The recirculating flow region decreases markedly with increasing leakage ratio.
- The velocity gradient of liquid in the recirculating flow region is not significantly influenced by the increasing leakage ratio.
- The recirculating flow is dispersed by the leakage flow at a leakage ratio of about 7% in the present experiment with a 21% corner blockage in water.

4.2 Rising bubble (Type 1)

The flow pattern Type 1 is characterized by gas bubbles rising up through the wake without forming a gas cavity. This is observed in the lower velocity range of the main flow. The dependence of rising velocity on axial position of the test section is shown in Fig. 11, where the position was measured at the bubble centre. The rising velocity increases in the axial direction and approaches the mean velocity of the main flow. Gas bubbles will be accelerated on entering the main stream. Between 6 and 7cm, however, the observed acceleration is small enough to be neglected in comparison with the acceleration above 7cm.

This shows that the influence of the main stream on the rising velocity is very small in this region, and suggests that the wake region near the wall extends only as far as 7cm for a main flow velocity of 1.2m/s. This compares well with the previous experiments [3].

The dependence of the rising velocity on the bubble size is shown in Fig. 12 for various leakage ratios. The flow distribution behind the blockage changes with increasing leakage ratio and then the path of the rising bubbles changes. In the figure the position of the measurement was between 6 and 7 cm downstream of the blockage,

independent of the leakage ratio.

The injected gas forms small bubbles, which then circulate behind the blockage. As described in [3], the circulating bubbles coalesce, forming a larger bubble which then rises up. With increasing leakage ratio, the circulating bubble region decreases in size and moves downstream. In the case of $\phi=0\%$, the rising bubbles are produced by coalescence at a position below the measuring point. However in the cases of $\phi=4$ and 8% , the bubbles directly rise up from the position of the gas injection without coalescence at the measuring point. The bubble becomes larger by coalescence. Hence the bubble size is largest for $\phi=0\%$ in comparison with other cases.

The acceleration of the bubble in the case of $\phi=0$ is large, as seen in Fig. 11. This may be due to the large size of the bubble. The bubble may cross the boundary between the main stream and the wake and enter the main stream due to its large size, resulting in a high acceleration by the main stream.

The solid curves in Fig. 12 were obtained from the calculation of rising velocities due to buoyancy in stagnant water. The rising velocity of a spherical gas bubble due to buoyancy can be expressed as follows [3].

$$v_g = v_l + \sqrt{\frac{8 r_b g}{3 C_D}} \quad (2)$$

where v_l is the liquid velocity, r_b is the bubble radius, g is the acceleration of gravity and C_D is the drag coefficient. In stagnant liquid, the rising velocity is then expressed as follows:

$$v_{g0} = \sqrt{\frac{8 r_b g}{3 C_D}} \quad (3)$$

The motion of gas bubbles in stagnant liquids has been studied by Peeble and Garber [11] and divided into four types. Two of the four types correspond to the viscous and transition regions

and the other two correspond to the turbulent region. The rising velocity can be calculated by using the drag coefficient equations presented by Peeble and Garber for these four regions. Though the data in Fig. 12 are scattered, especially in the case of $\phi=0$, it may be seen that the experimental results are consistent with the calculation, even at $\phi=8\%$. The gas is separated from the region behind the blockage due to buoyancy in the lower velocity range of the main flow and in the higher range of the leakage ratio.

Above a leakage ratio of 7%, there is no recirculating flow behind the blockage. The agreement between the calculation and experiments at $\phi=8\%$ in Fig. 12 suggests that the liquid velocity behind the blockage is relatively low even after the disappearance of the recirculating flow. When the main flow velocity is 1.2m/s, the mean velocity of the leakage flow of $\phi=8\%$ through the blockage is about 0.1m/s. The rising velocity of bubbles for $\phi=8\%$ is about 0.3m/s, as shown in Fig. 12. The leakage ratio at which the mean velocity of the leakage flow becomes comparable with the rising velocity is about 25% for a main flow velocity of 1.2m/s.

4.3 Gas cavity (Type 2)

The flow pattern Type 2 is characterized by a stationary gas cavity formed in the wake. This is observed in a distinct velocity range of the main flow.

The change of the flow pattern Type 2 to Type 1 by the increase of the leakage ratio is schematically shown in Fig. 13 and photographs in Fig. 14.

At $\phi=0$, the large gas cavity is present behind the blockage. At $\phi=4\%$, the gas cavity still remains but its size becomes small. At $\phi=6\%$, the small bubbles circulate in the limited area near the stagnation point and no cavity can be seen. The bubbles coalesce in the recirculating flow region, forming a larger bubble which then rises up. At $\phi=8\%$, the bubbles rise up without circulation because no recirculating flow exists behind the blockage.

The dependence of the cavity size on the leakage ratio is shown in Fig. 15, where the size is represented with effective radius expressed as follows [3]:

$$r_c = \frac{1}{2} \sqrt{a \cdot b}$$

where a is the width and b is the height of cavity which can be measured in the photographs. The cavity radius decreases steadily at first as the leakage ratio increases, being halved in size for a leakage ratio of about 5%. At this value of leakage ratio, a sharp reduction in cavity size is observed, and at higher leakage ratios no cavity exists. This may be due to buoyancy. As described in [3], a gas cavity cannot remain in the wake, but rises up as a single bubble due to buoyancy in the lower velocity range of the main flow. The decrease of the main flow velocity causes a decrease of the maximum velocity of the reverse flow near the wall. The increase of the leakage ratio also causes a decrease of the maximum reverse flow velocity, as shown in Table 2. Hence the gas cavity rises up as a single bubble by buoyancy at the higher leakage ratios.

The residence time is defined as the time from the termination of gas injection to the disappearance of the cavity. The residence time depends strongly on the main flow velocity, decreasing with increasing velocity [3]. The dependence of the residence time on the leakage ratio is shown in Fig. 16, where the gas injection rate before termination is given because the initial cavity size increases with increasing gas injection rate. The residence time decreases with increasing leakage ratio and falls to zero at a leakage ratio of about 5%.

5. Dispersion of gas cavity

5.1 Critical velocities for cavity formation

The influence of the leakage ratio on the gas cavity region is shown in Fig. 17. The lines represent the boundaries of the region where a gas cavity was observed. The main flow velocities at the boundaries are called "critical velocities" for gas cavity formation.

The influence of the leakage ratio on these critical velocities is shown in Fig. 18 for a constant gas injection rate. From Figs. 17 and 18, the following can be stated:

- The upper critical velocity is independent of the leakage ratio.
- The lower critical velocity increases with increasing leakage ratio and finally meets the upper critical velocity.

The leakage ratio at which the two critical velocities meet is called the "critical leakage ratio" for gas cavity dispersion. Above the critical leakage ratio no gas cavity is present behind the blockage.

5.2 Critical leakage ratio for cavity dispersion

The dependence of the critical leakage ratio on gas injection rate is shown in Fig. 19, where the bar represents the range of uncertainty of data. With increasing gas injection rate the critical leakage ratio increases gradually, showing only a weak dependence, and then reaches a maximum value. So the critical leakage ratio for gas cavity dispersion is independent of gas injection rate at rates above $20 \text{ Ncm}^2/\text{s}$.

In the case of the present experiment with a 21 % corner blockage in water, the critical leakage ratio is about 5 %. The critical leakage ratio may, however, depend on blockage fraction and location.

5.3 Mechanisms of gas cavity dispersion

The gas cavity is sustained by the effects of gas accumulation and of cavity breakup. These rates of accumulation and breakup depend on the liquid velocities in the wake. With increasing main flow velocity, the liquid velocities in the wake increase and then the cavity size decreases, giving the minimum value ($r_c = 2.7$ mm) at the upper critical velocities.

Though the recirculating flow region decreases with increasing leakage ratio, the liquid velocities in the region are not significantly changed, as mentioned in Section 4.1. Hence, the independence of the upper critical velocity may be due to the insensitivity of the liquid velocity gradient in the recirculating flow region to the leakage flow.

The increase of the lower critical velocity may be due to the decrease in size of the recirculating flow region. Bubbles are separated from the liquid behind the blockage due to buoyancy, in the lower velocity range of the main flow. The decrease in size of the recirculating flow region leads to a decreased maximum reverse flow velocity, so that a higher main flow velocity is required to prevent the escape of bubbles due to buoyancy.

Therefore, the gas cavity dispersion behind a porous blockage is due to buoyancy and the reduction in size of the recirculating flow region by the leakage flow. The critical leakage ratio for gas cavity dispersion (~ 5 % in the present experiment) is lower than the critical leakage ratio for the dispersion of the recirculating flow (~ 7 %), because of the separation of gas from the liquid by buoyancy.

6. Theoretical analysis

In the lower velocity range of the main flow, the circulating velocity of the liquid in the wake is relatively small. Hence, the motion of bubbles in the wake due to buoyancy is discussed on the assumption that the influence of the other flow forces such as the centripetal force or pressure fluctuations described in [12] can be neglected, and the critical leakage ratio for gas cavity dispersion is analytically predicted in this section.

6.1 A flow model

To account for the bubble motion in the wake behind a blockage, a simple model of the wake structure is required. Such a model was made [12] to consider the mechanisms of gas cavity break-up behind an impermeable blockage after the termination of gas injection. In the present report, the model developed in [12] is extended to a porous blockage case and the bubble motion in the wake is discussed.

6.1.1 Features of the model

6.1.1.1 Flow distribution behind an impermeable blockage

The model of the wake structure for an impermeable blockage, developed in [12], is briefly repeated. The model is schematically shown in Fig. 20, where the main coolant flow is upwards.

The main stream velocity increases in the axial direction of the subassembly due to the flow obstruction and reaches a maximum value at the leading edge of the blockage, then decreasing to a mean velocity in the subassembly.

The liquid in the wake flows down near the wall from the stagnation point to the separation point at the blockage edge (i.e. reverse flow), then entering the main stream. The liquid between the main stream and reverse flow near the wall rotates and forms a vortex.

The existence of such a vortex is assumed and called a "central vortex". The central vortex is a limited region within the wake behind a blockage.

The velocity and turbulence in the wake on the main stream side are different from those on the subassembly wall side. Hence, the central vortex is divided into two regions: Region 1 on the main stream side and Region 2 on the wall side. The velocity and turbulence of the flow in Region 1 are higher than those in Region 2.

For the velocity distribution in each region of the vortex, the following assumption was made.

- The angular velocity distribution of liquid is uniform within each region, but the magnitude is different.

6.1.1.2 Flow distribution behind a porous blockage

The model for an impermeable blockage is extended to a porous blockage case. The extended model of the flow distribution behind a porous blockage is schematically shown in Fig. 21. In the model, the area behind the blockage is divided into two regions: recirculating flow region and leakage flow region. As mentioned in Section 4.1, the distance between the recirculating flow region and the blockage increases significantly with increasing leakage ratio, whereas the stagnation point moves downstream only slightly.

A gas cavity may be formed in the central vortex in the recirculating flow region and then rise up as a single bubble due to buoyancy. To predict the critical leakage ratio for the gas cavity dispersion, the motion of the bubble in the central vortex is discussed.

Then two models may be possible: a "floating-centre" model and "fixed-centre" model. A comparison between these models is schematically shown in Fig. 22. In the case of floating-centre model the position of the vortex centre moves upwards with increasing leakage ratio and simultaneously the vortex radius decreases. If the observation point moves with the centre of the vortex the change in the vortex radius is observed.

In the case of the fixed-centre model only the vortex radius decreases with the increasing leakage ratio. In the present report, the fixed-centre model is used to discuss the motion of the bubble in the vortex, because it allows discussion of the bubble motion without taking account of the change of the location of the vortex centre behind the blockage.

6.1.1.2 Velocity distribution in the vortex

The fixed-centre model for calculations of the bubble motion in the central vortex is schematically shown in Fig. 23. On the assumption of uniform angular velocity distribution, the tangential velocity of liquid in Region 2 of the central vortex is expressed as follows:

$$v = r \cdot \omega \quad (4)$$

where r is the radial position in the vortex and ω is the angular velocity. The reverse flow velocity at the vortex edge of Region 2 is expressed as follows:

$$v_u = r_w \cdot \omega \quad (5)$$

where r_w is the vortex radius, which depends on leakage ratio.

The reverse flow velocity for an impermeable blockage ($\phi = 0$) is also expressed as follows:

$$v_{u0} = r_{w0} \cdot \omega \quad (6)$$

where r_{w0} is the vortex radius for an impermeable blockage, which is expressed as a function of blockage size as follows [12]:

$$r_{w0} = \frac{1}{2} \sqrt{\frac{A_{bf} \xi_w}{\pi}} \quad (7)$$

where A_{bf} is the blockage area including fuel pins and ξ_w is a geometrical factor which is equal to 3 ($= 360^\circ/120^\circ$) in the corner blockage case. For the present experiment, a value of 6 ($= 360^\circ/60^\circ$) must be used for ξ_w because the test section used is a half size of the subassembly. The vortex radius is about 21 mm in the present case. The reverse flow velocity near the wall is related to the main flow velocity as follows:

$$v_{w0} = \varepsilon \cdot v_0 \quad (8)$$

where v_0 is the main flow velocity and ε is the ratio of the maximum reverse flow velocity to the main flow velocity. From Eqs. (6) and (8), the angular velocity is expressed as follows:

$$\omega = \varepsilon \cdot \frac{v_0}{r_{w0}} \quad (9)$$

If the vortex centre is adopted as the origin of x and y coordinates, the radial position in the vortex is expressed as follows:

$$r = \sqrt{x^2 + y^2} \quad (10)$$

Then the tangential velocity is rewritten from Eq. (4) as follows:

$$v = \sqrt{x^2 + y^2} \cdot \omega \quad (11)$$

6.1.3 Change of vortex radius

The dependence of the vortex radius on leakage ratio is assumed to be linear and expressed as follows:

$$r_w = r_{w0} - \frac{r_{w0}}{\phi_w} \cdot \phi \quad (12)$$

where ϕ_w is the leakage ratio at which the recirculating wake disappears behind a blockage. The leakage ratio may depend on blockage geometry. The leakage ratio for wake dispersion for the present experiment is about 7%, was mentioned in section 4.1.

6.2 Bubble motion due to buoyancy in the vortex

The motion of the bubble due to buoyancy in the vortex is considered. The position of the bubble in the vortex is represented by (X, Y) . In the X -direction there is no relative velocity between the liquid and the bubble but in the Y -direction due to buoyancy. The X - and Y -components of the bubble velocity in the vortex are respectively expressed as follows:

$$\frac{dx}{dt} = v \cdot \cos \theta \quad (13)$$

$$\frac{dy}{dt} = v_{g0} - v \cdot \sin \theta \quad (14)$$

where v_{g0} is defined by Eq. (3) and where

$$\sin \theta = \frac{x}{\sqrt{x^2 + y^2}}, \quad \cos \theta = \frac{y}{\sqrt{x^2 + y^2}} \quad (15)$$

By substituting Eq. (15) into Eqs. (13) and (14) and using Eq. (11), the following equations are obtained.

$$\frac{dx}{dt} = y \cdot \omega \quad (16)$$

$$\frac{dy}{dt} = v_{g0} - x \cdot \omega \quad (17)$$

From Eqs. (16) and (17) the following equation is obtained.

$$\frac{dy}{dx} = \frac{U_{g0} - X \cdot \omega}{y \cdot \omega} \quad (18)$$

By integrating Eq. (18) the following equation is obtained.

$$(\omega x - U_{g0})^2 + (\omega y)^2 = (U_{g0})^2 \quad (19)$$

where $y=0$ at $x=0$. The motion of the bubble in the vortex due to buoyancy can be calculated by Eq. (19) and is shown in Fig. 24, where the rising velocity due to buoyancy in stagnant water was assumed to be 0.3m/s. The gas cavity is formed in the vortex but rises up as a single bubble due to buoyancy. Hence, it is assumed that the bubble starts to move from the centre of the vortex. The trajectory of the bubble is circular. With increasing angular velocity of the liquid, the radius of the trajectory is decreased.

As seen in the figure the bubble can escape from the vortex if the angular velocity is less than about 30 sec^{-1} . With increasing angular velocity the downward velocity of liquid against the rising bubble increases and finally the bubble goes down with the liquid, resulting in the retention of gas in the vortex.

It is found that the bubble can easily escape from the wake in the case of a porous blockage, even in the higher angular velocity range, since the vortex radius is decreased with the increasing leakage ratio.

6.3 Prediction of critical leakage ratio

The critical condition for gas separation from the liquid in the vortex due to buoyancy is expressed as follows:

$$\frac{dy}{dt} = 0 \quad \text{at} \quad r = r_w \quad (20)$$

When $d\eta/dt > 0$ at $r = r_w$, the bubble can escape from the wake. When $d\eta/dt < 0$ at $r = r_w$, the bubble is captured in the vortex. Therefore, equation (20) may be related to the critical velocity of the lower boundary for gas cavity formation, and hence with the critical leakage ratio for cavity dispersion.

From Eqs. (10), (17), (19), and (20) the following equation is obtained.

$$\sqrt{2} \cdot v_{g0} = r_w \cdot \omega \quad (21)$$

From Eqs. (9), (12), and (21) the lower critical velocity is expressed as follows:

$$(v_0)_{\text{lower}} = \frac{\sqrt{2} \cdot v_{g0}}{\epsilon} \cdot \frac{\phi_w}{\phi_w - \phi} \quad (22)$$

The rising velocity depends on bubble size, as shown in Fig. 12. However, the rising velocity is treated as a constant for the calculation of the critical velocity. The ratio of the maximum reverse flow velocity to the main flow velocity may depend on the main flow velocity. However, this ratio is also treated as a constant for the calculation. Then the lower critical velocity can be calculated by Eq. (22).

A comparison between measured and calculated lower critical velocities is shown in Fig. 25, where a velocity of 0.3 m/s was used for the rising velocity in stagnant water. Taking account of the change of the ratio, ϵ , with increasing main flow velocity, it can be said that the calculated values are in good agreement with the measured values.

The critical leakage ratio for gas cavity dispersion is defined as follows:

$$\phi = \phi_c \quad \text{for} \quad (v_0)_{\text{lower}} = (v_0)_{\text{upper}} \quad (23)$$

where $(v_0)_{\text{upper}}$ is the upper critical velocity which depends on the gas injection rate. From Eqs. (22) and (23) the critical leakage ratio for cavity dispersion is expressed as follows:

$$\phi_c = \phi_w \cdot \left(1 - \frac{\sqrt{2} \cdot v_{ho}}{\epsilon \cdot (v_0)_{\text{upper}}} \right) \quad (24)$$

A comparison between measured and calculated values of the critical leakage ratio for gas cavity dispersion is shown in Fig. 26, where the experimental results of the upper critical velocity were used for the calculation. In the limited range of available data, it can be said that calculated values show good agreement with the measured values.

It is concluded that buoyancy and the reduction of the vortex size with increasing leakage ratio are of importance for the gas cavity dispersion behind a porous blockage. The reduction of the maximum reverse flow velocity is accompanied by the reduction in size of the recirculation zone, allowing gas bubbles to escape easily from the vortex by buoyancy.

7. Transient conditions

7.1 Release rate of fission gas from a fuel pin

The release rate of fission gas from a fuel pin is estimated. The release rate depends on gas plenum pressure, rupture size and friction factor in the pellets of the pin. In the special case that the gas is released with sonic velocity or ultra-sonic velocity, the release rate gives a maximum, i.e. choking flow. On the assumption of the isentropic expansion, the maximum gas release rate due to the choking flow is expressed as follows:

$$M_{g,max} = A_t \cdot P_g \cdot \sqrt{\frac{\gamma}{R_g T_g} \left(\frac{2}{\gamma+1}\right)^{\frac{\gamma+1}{\gamma-1}}} \quad (25)$$

where T_g and P_g are the temperature and pressure in the gas plenum, respectively, γ is the ratio of the specific heats and A_t is the throat area. Adopting the rupture area as the throat area, A_t is expressed as follows:

$$A_t = \pi \left(\frac{d_r}{2}\right)^2 \quad (26)$$

where d_r is the effective diameter of rupture area.

The mass flow rate is related with the volumetric release rate under standard conditions as follows:

$$V_{g,max} = M_{g,max} \cdot \left(\frac{R_g T_0}{P_0}\right) \quad (27)$$

where T_0 and P_0 are the standard temperature and pressure (0 °C, 1 bar). From Eqs. (25), (26), and (27), the following equation is obtained.

$$V_{g,max} = \left(\frac{R_g T_0}{P_0}\right) \pi \left(\frac{d_r}{2}\right)^2 P_g \sqrt{\frac{\gamma}{R_g T_g} \left(\frac{2}{\gamma+1}\right)^{\frac{\gamma+1}{\gamma-1}}} \quad (28)$$

The dependence of the maximum release rate on the gas plenum pressure under various rupture sizes is shown in Fig. 27, where Xenon was assumed as the fission gas and the value of γ equal to 5/3 was adopted. As shown in the figure the release rate of fission gas from a fuel pin has a wide range, depending on the gas plenum pressure and rupture size. Under transient conditions of fuel pin rupture in the subassembly of LMFBR, the release rate changes with time corresponding to the decrease of the gas plenum pressure.

7.2 Pulsewise gas injection

The gas was pulsewisely injected from a gas plenum into the flow behind the blockage to simulate a fuel pin rupture in an LMFBR subassembly, and the behaviour of gas was observed using high-speed cine film.

The behaviour of gas behind the blockage with a leakage ratio of 6 %, which is higher than the critical leakage ratio for cavity dispersion, is shown in Fig. 28, where the solid line represents the boundary of the two-phase mixture (bubbly) and the dotted circle represents a large bubble. As shown in the figure, the injected gas sometimes forms a large bubble behind the blockage, but the bubble rises and is then broken up into small bubbles.

No gas cavity is formed behind the blockage above the critical ratio in the pulsewise gas injection case as well as in the steady state injection case.

8. Conclusions

The behaviour of gas is significantly influenced by the leakage flow through the blockage. The changes in the recirculating flow region and liquid velocities are of importance for the behaviour of gas behind the blockage.

A gas cavity was formed behind the blockage under some experimental conditions. The size and the residence time of the gas cavity decreases with increasing leakage ratio. Above a leakage ratio of about 5%, a gas cavity was not observed behind a 21% corner blockage for any gas injection rate in the present experiments.

A simple flow model was developed and the critical leakage ratio for gas cavity dispersion predicted. The calculated values showed a good agreement with experimental results under the steady state gas injection. The gas cavity is dispersed by the reduction in size of the central vortex and by buoyancy.

Above the critical leakage ratio, no gas cavity is formed behind the blockage in the pulsewise gas injection case as in the steady state gas injection case.

Acknowledgement

The author would like to express his gratitude to Dr. W. Peppler and Mr. F. Huber for their valuable suggestions and discussions. The author wishes to express his thanks to Mr. G. Ochs and Mr. E. Jenes for their technical assistance.

Nomenclature

A_B	:	Blocked area of main flow.
A_{Bf}	:	Blockage area including fuel pins.
A_0	:	Total area for main flow.
A_t	:	Throat area for released gas flow.
C_D	:	Drag coefficient.
M_B	:	Mass flow rate through the blockage.
M_0	:	Total mass flow rate through the subassembly.
M_{g-max}	:	Maximum release rate of gas.
P	:	Pressure.
R_g	:	Gas constant.
T	:	Temperature.
V_{g-max}	:	Maximum volumetric release rate under standard conditions
a	:	Width
b	:	Height
d_r	:	Effective diameter of rupture area
g	:	Acceleration due to gravity
r	:	Radial position
r_b	:	Bubble radius
r_c	:	Gas cavity radius
r_w	:	Vortex radius
t	:	Time
v	:	Velocity
v_0	:	Main flow velocity
v_{g0}	:	Rising velocity due to buoyancy in stagnant liquid
v_u	:	Reverse flow velocity near the wall
x, y	:	Positions in the central vortex
γ	:	Ratio of specific heats
ϵ	:	Ratio of the maximum reverse flow velocity to the main flow velocity
θ	:	Angle
ϕ	:	Leakage ratio
ϕ_c	:	Critical leakage ratio for cavity dispersion
ϕ_w	:	Critical leakage ratio for wake dispersion
ω	:	Angular velocity

Suffix

g	:	Gas
l	:	Liquid

References

- [1_] Status of LMFBR Safety Technology
1. Fission Gas Release in Reactor Safety
CSNI Report No. 40 (November 1979)
- [2_] A.J. Clare, F. Huber, W. Till and W. Pepler
"Preliminary Results of the Temperature Distribution and Boiling Behaviour behind a Wall Blockage in a 169 Pin Bundle"
8. Liquid Metal Boiling Working Group Meeting / Mol
(Oct. 1978)
- [3_] Y. Fukuzawa
"Observations of the Behaviour of Gas in the Wake behind a Corner Blockage in Fast Breeder Reactor Subassembly Geometry"
KfK 2820 (July 1979)
- [4_] P. Basmer, D. Kirsch and G.F. Schultheiß
"Phänomenologische Untersuchungen der Strömungsverteilung hinter lokalen Kühlkanalblockaden in Stabbündeln"
KfK 1548 (Jan. 1972)
- [5_] D. Blackburn, R.J. Butterfield, A. Edwards and G. Nash
"Local Blockage Studies in Fast Reactor Sub-Assemblies using the SABRE Code"
The 6'th Meeting of LMBWG, Risley (Oct. 1975)
- [6_] C.V. Gregory and D.J. Lord
"Effect of Permeability on the Consequences of Local Blockages in Fast Reactor Subassemblies"
J. Br. Nucl. Energy Soc., Vol. 15, No. 1, p.53-60,
(Jan. 1976)
- [7_] A.M. Judd
"Measurement of Flow in an Air Model of a Partly Blocked Fast Reactor Subassembly"
J. Br. Nucl. Energy Soc., Vol. 15, No. 1, p.47-52
(Jan. 1976)

- ┌⁻8_┐ D.P. Robinson
"Water Modelling Studies of Blockages with Discrete
Permeabilities in an 11 Pin Geometry"
AEEW-M 1484 (June 1977)
- ┌⁻9_┐ Y. Fukuzawa: not published
- ┌⁻10_┐ R. Zahoransky: not published
- ┌⁻11_┐ F.N. Peebles and H.J. Garber
"Studies on the Motion of Gas Bubbles in Liquids"
Chemical Engineering Progress, Vol. 49, No. 2, pp.88-97
- ┌⁻12_┐ Y. Fukuzawa
"A Model of Gas Cavity Breakup behind a Blockage in Fast
Breeder Reactor Subassembly Geometry"
KfK 2953 (May 1980)

Table 1 Leakage ratio for the dispersion of circulating bubbles

Main flow velocity [\bar{m}/s]	3.0	3.5	4.0	4.5
Leakage ratio [%]	6.7	6.7	6.8	6.8

Table 2 Reverse flow velocity near the wall (average values)

Leakage ratio [%]	0	1.5	3.0	4.0	5.0	6.0
Reverse flow velocity [\bar{m}/s]	1.1	0,8	0.7	0.5	0.4	0.1

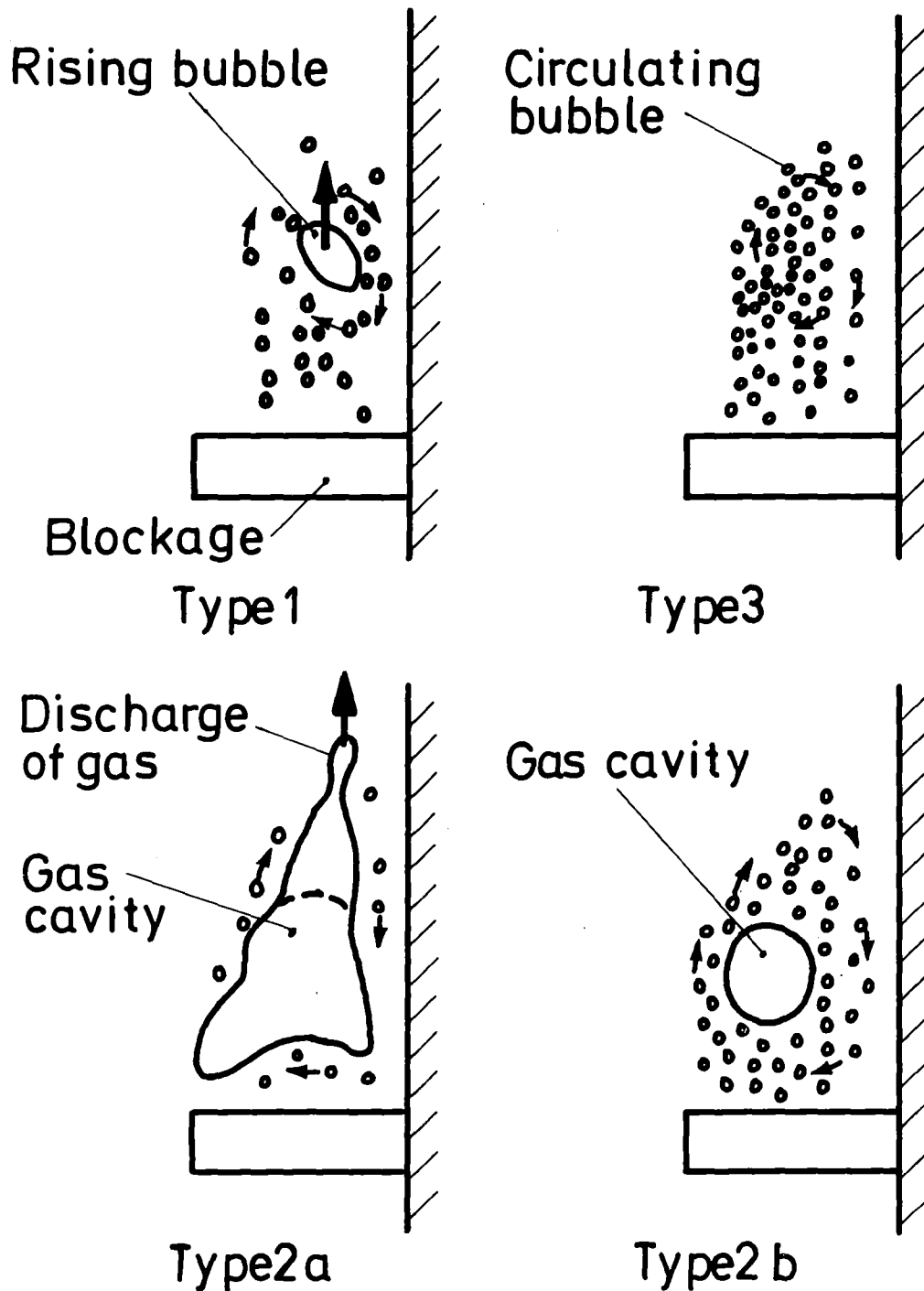
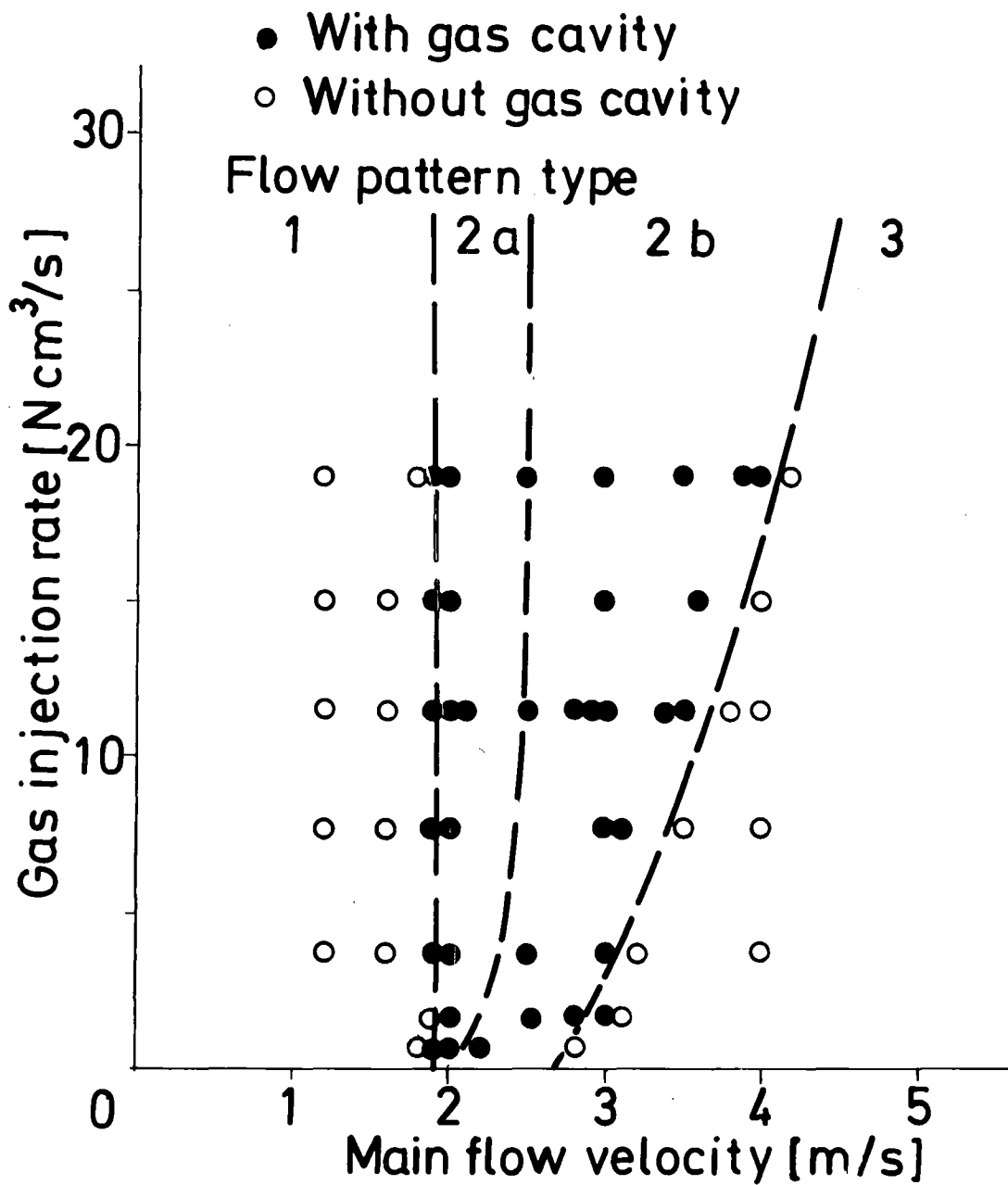


Fig.1 Schematic diagrams of two-phase flow patterns in the wake behind an impermeable blockage [3]



Downstream gas injection



Fig.2 Relation between flow pattern, gas injection rate and main flow velocity for an impermeable blockage [3]

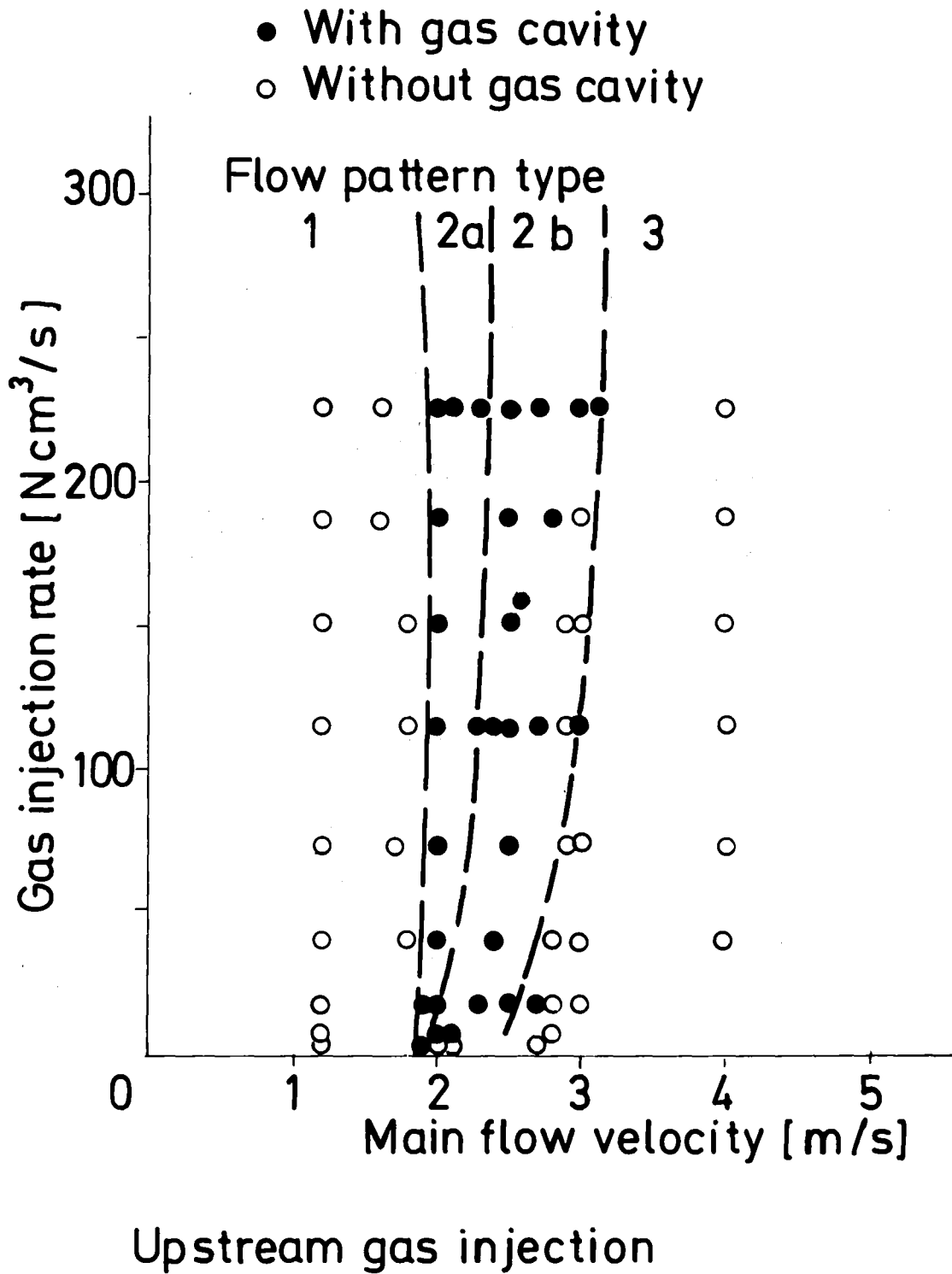
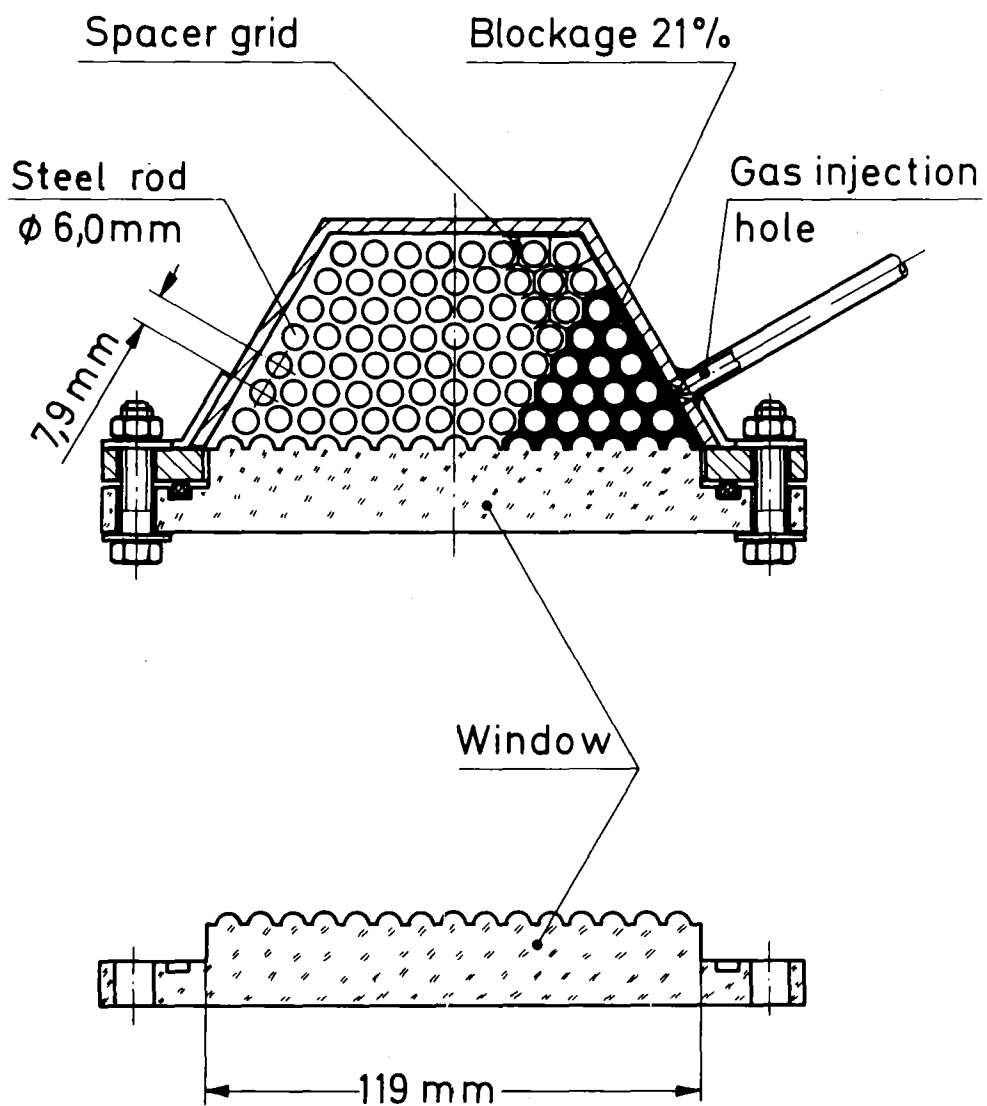


Fig. 3 Flow pattern for an impermeable blockage [3] dependent on gas injection rate and main flow velocity



KIK

Fig.4 Cross section of test section

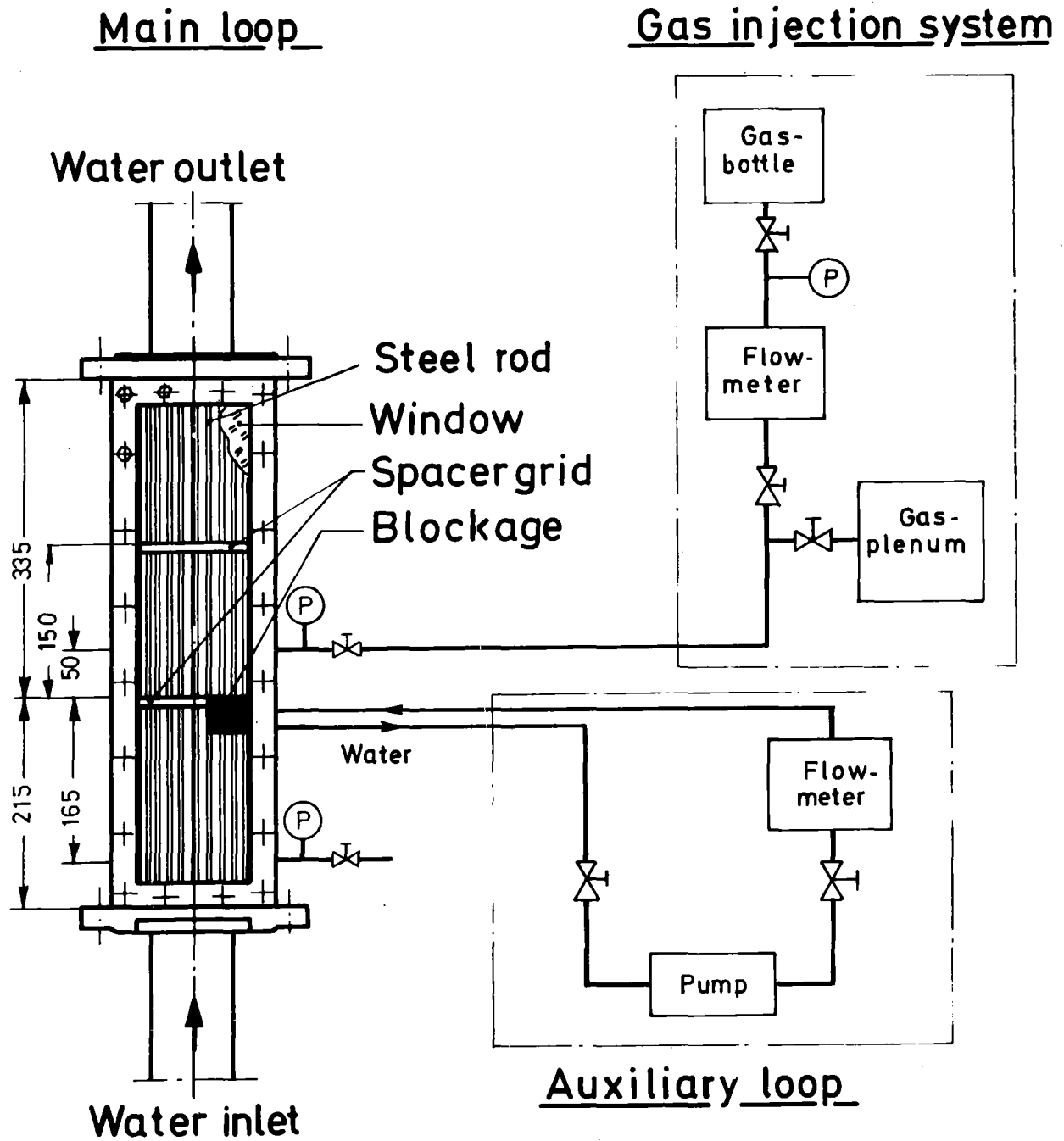


Fig.5 Schematic view of the experimental set up

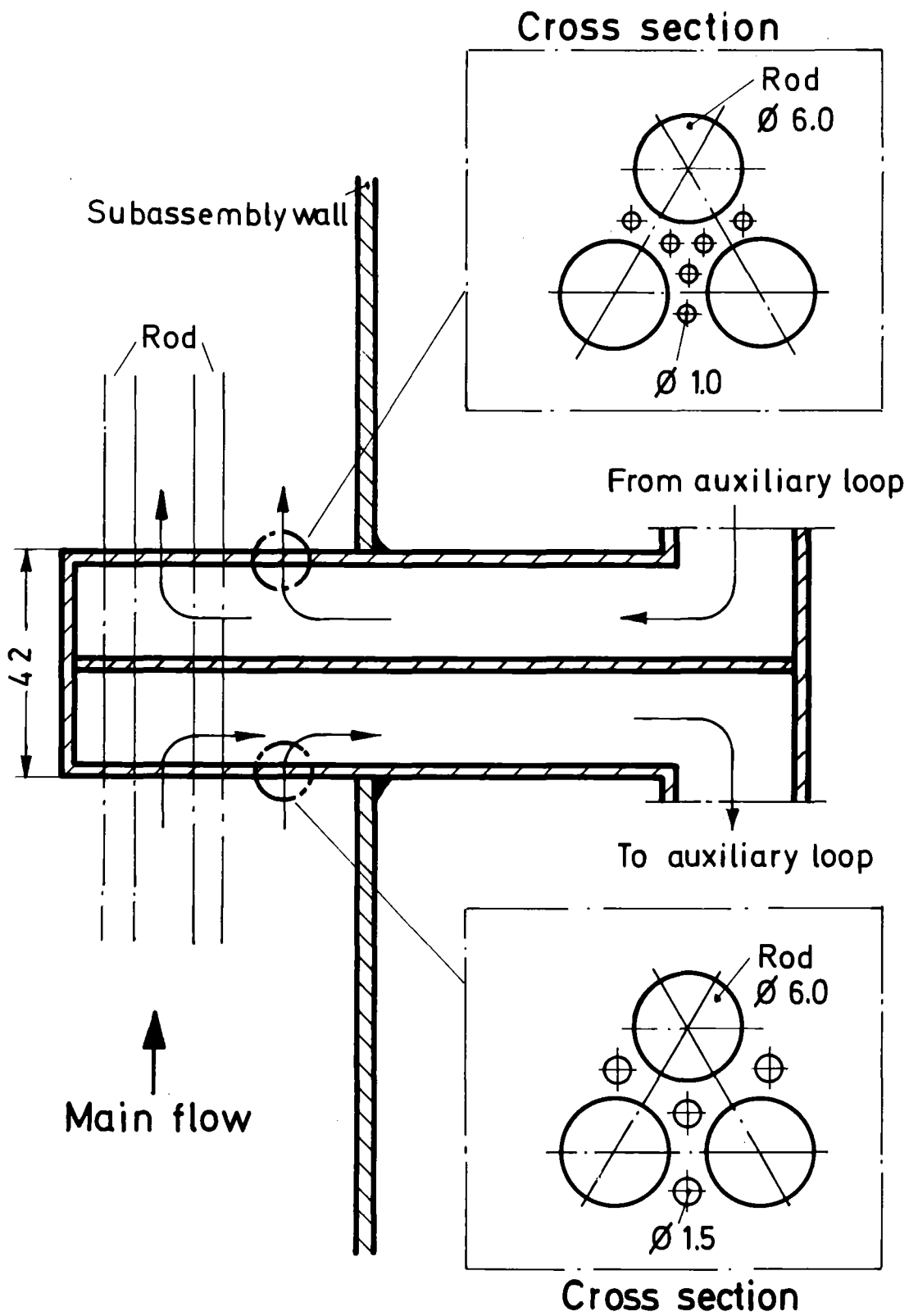


Fig.6 Blockage geometry axial view

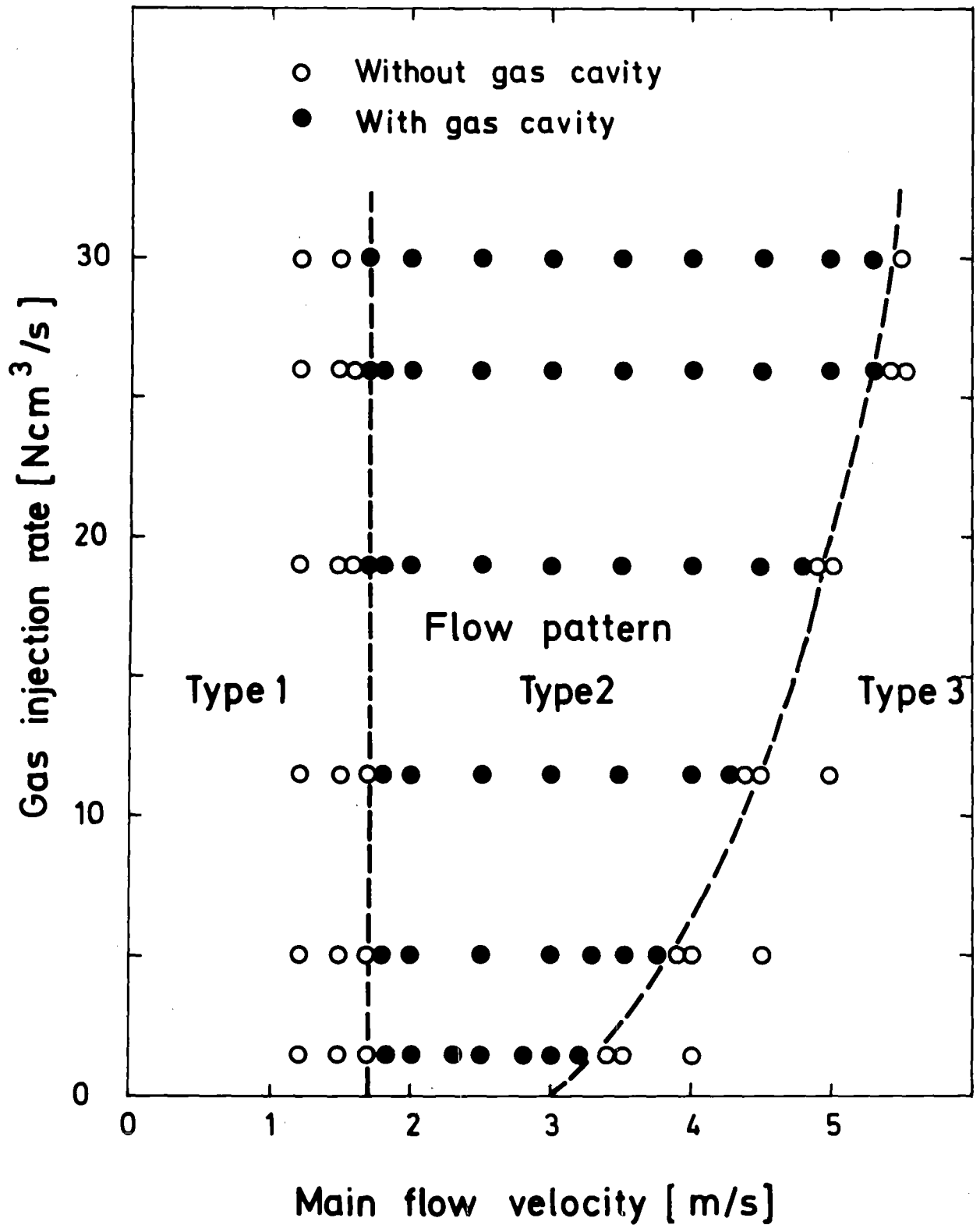


Fig.7 Relation between gas injection rate, main flow velocity and flow pattern types for the blockage with no leakage flow

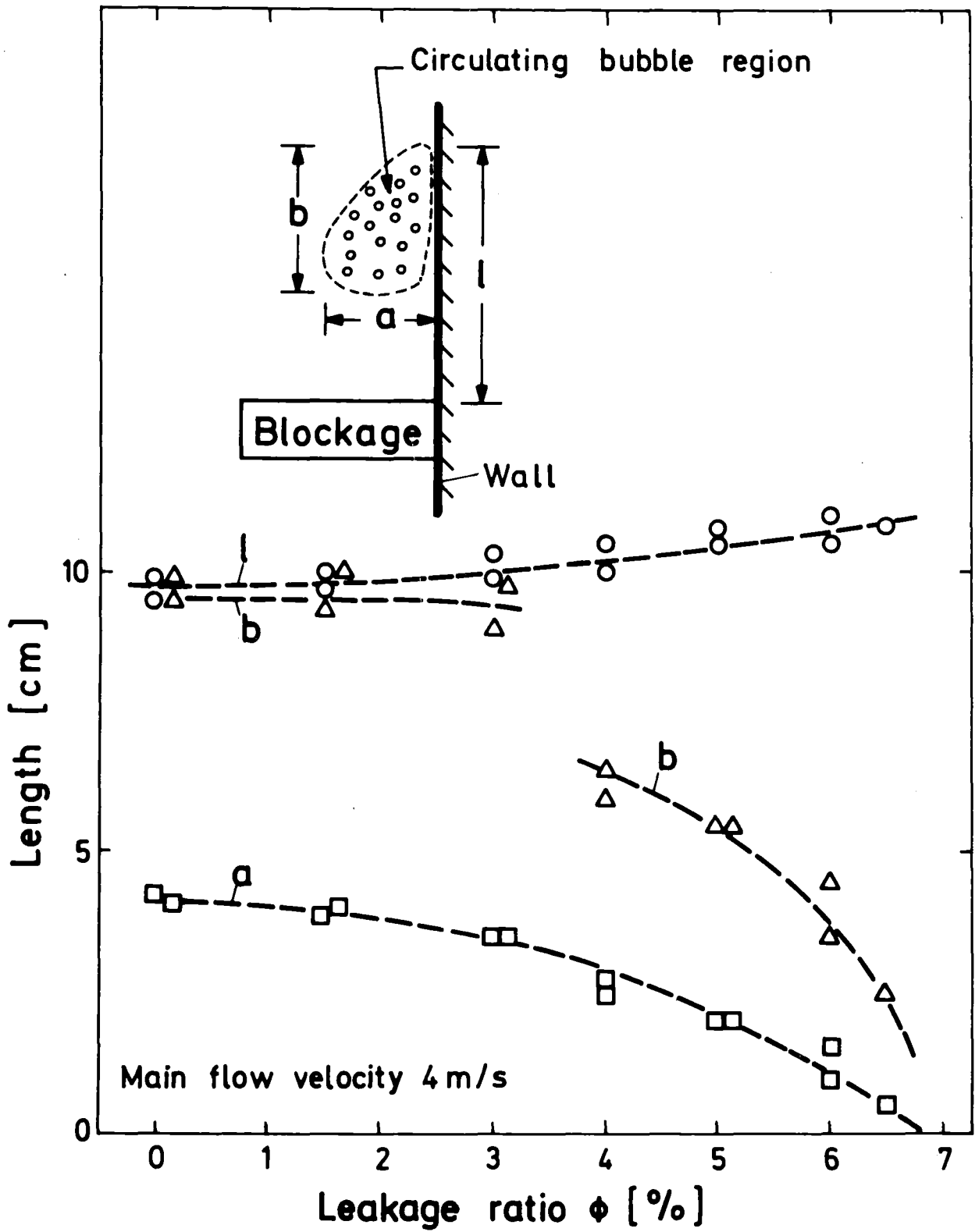


Fig.8 Change of circulating bubble region behind the blockage

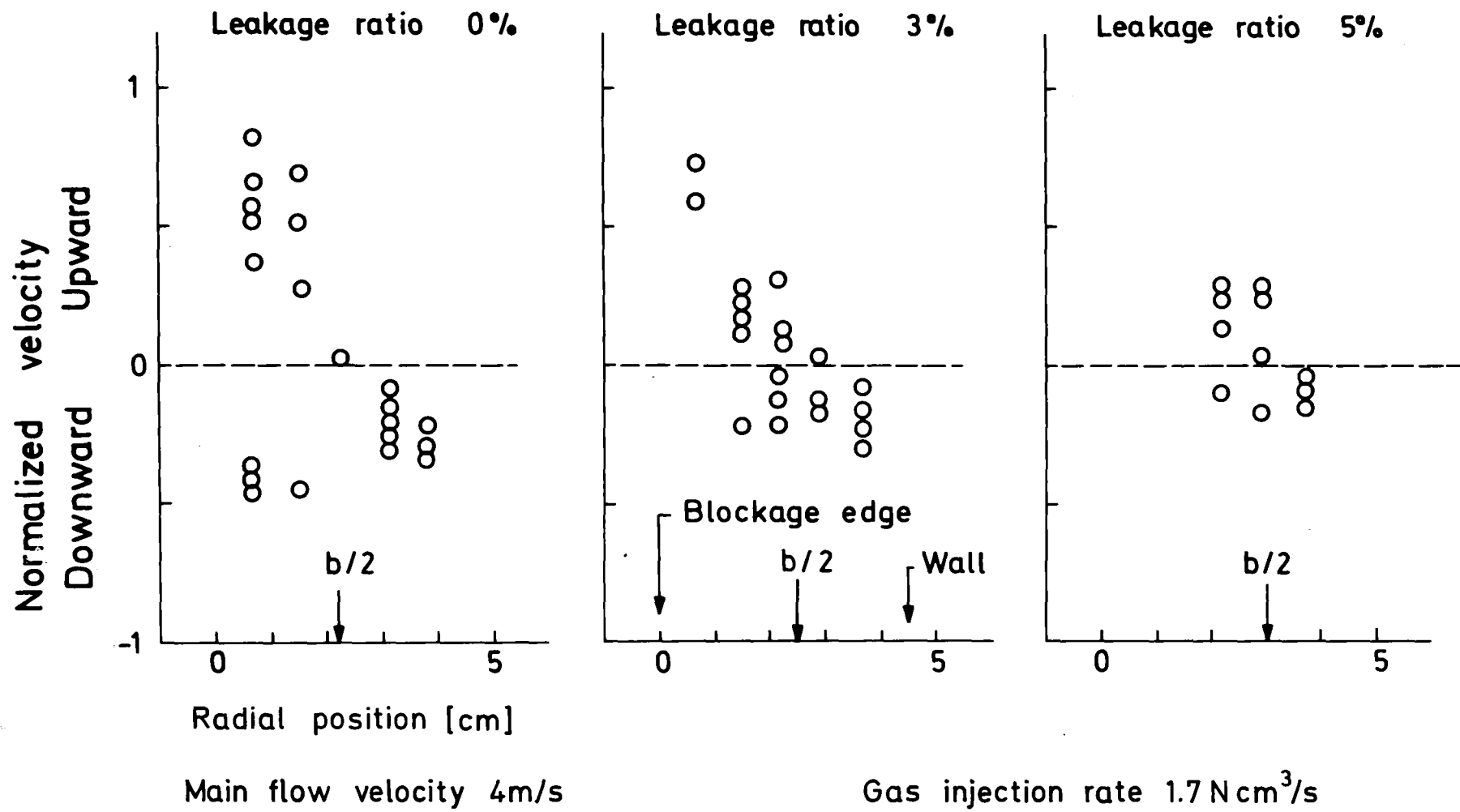
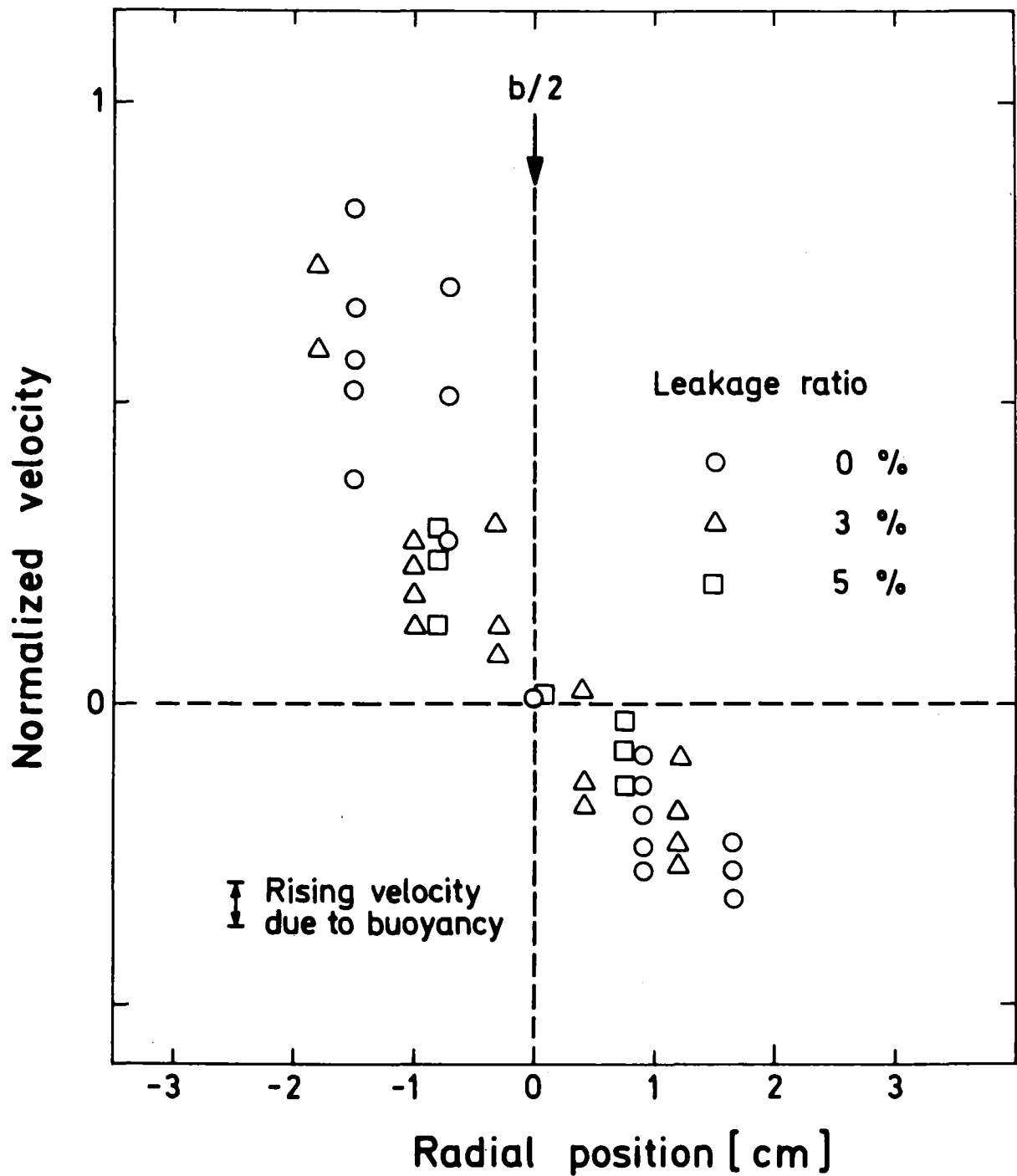


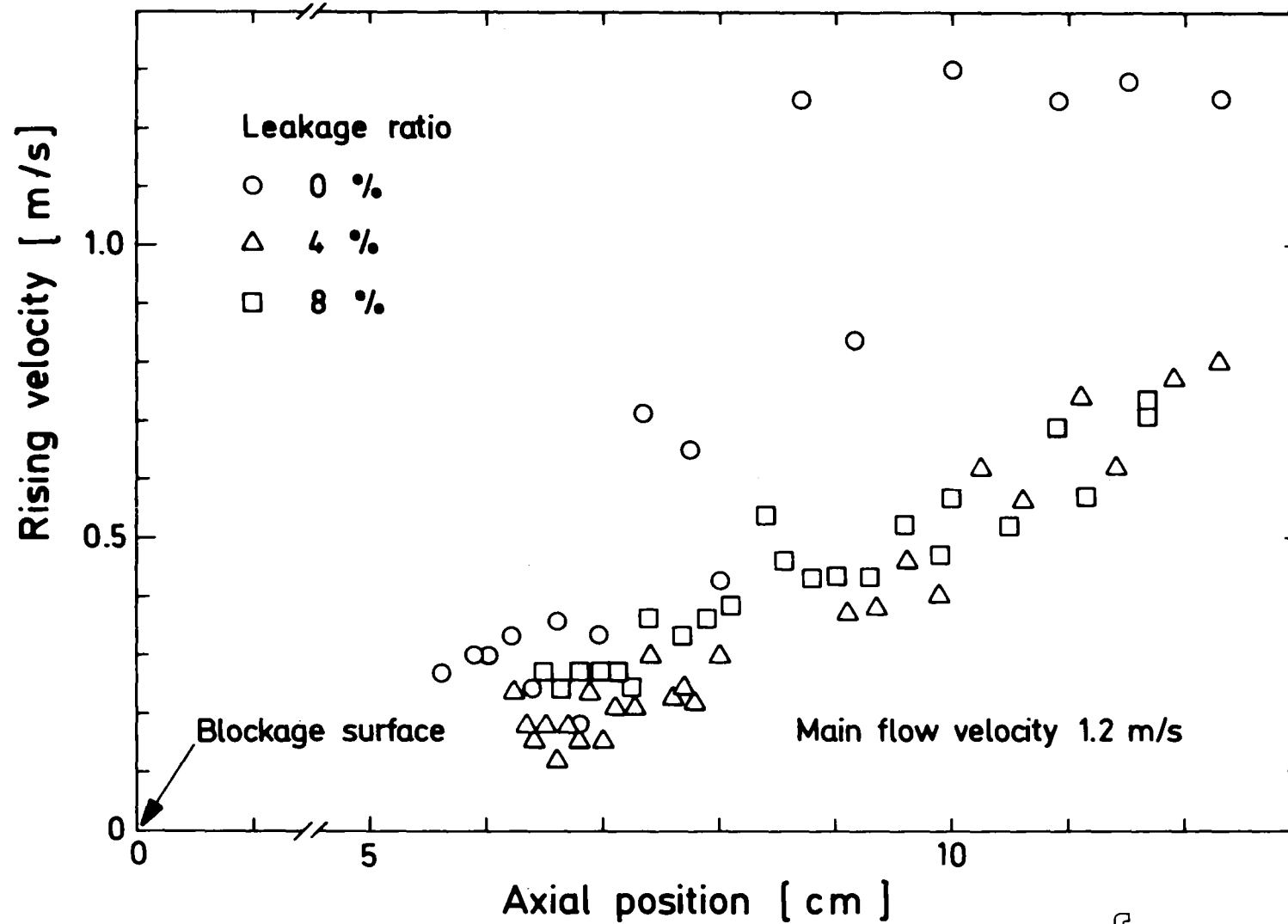
Fig.9 Radial distribution of axial velocity of bubbles for various leakage ratios



Main flow velocity 4 m/s

KJK

Fig.10 Comparison of bubble velocity distributions for various leakage ratios



KIK

Fig.11 Dependence of rising velocity on axial position

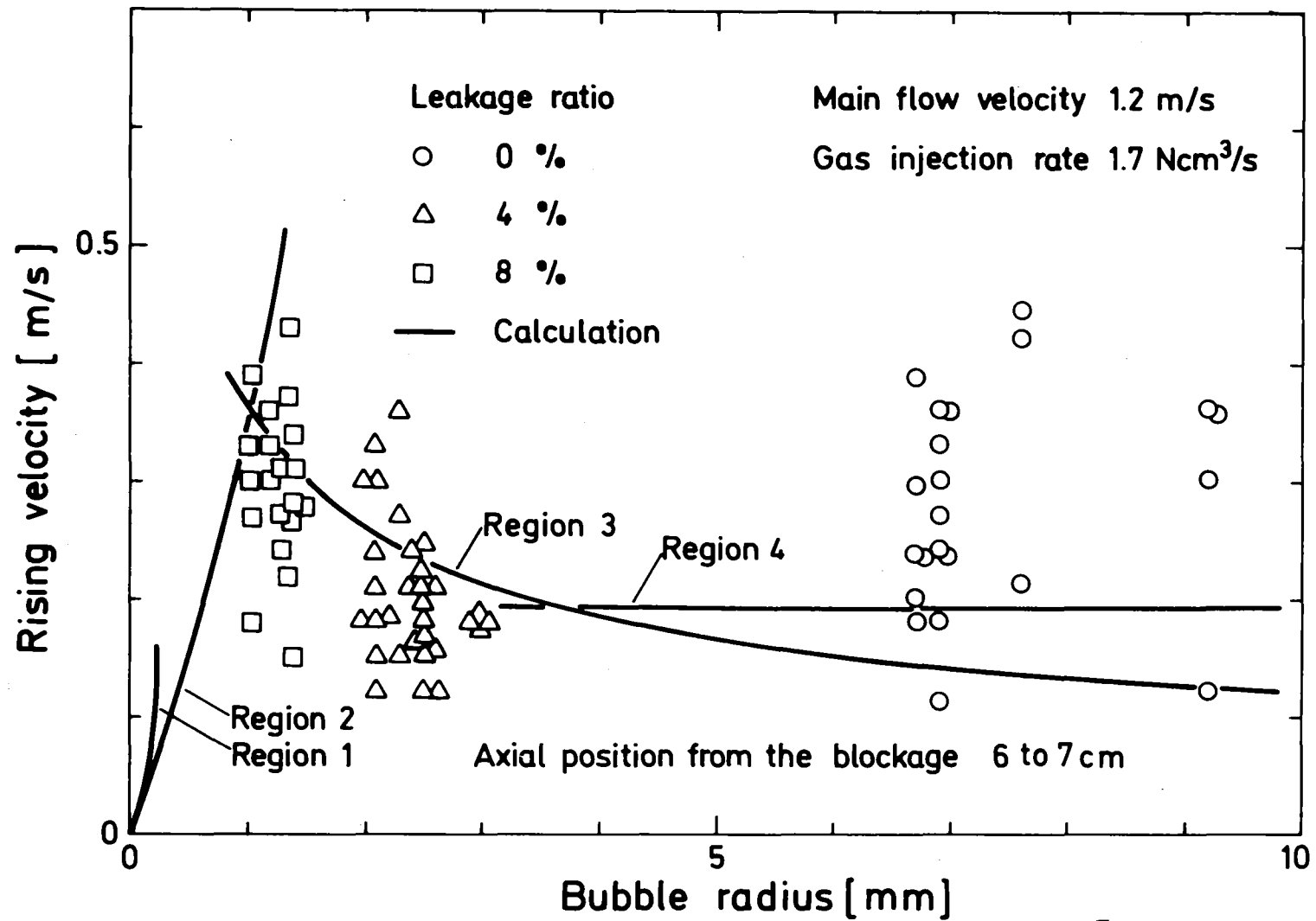


Fig.12 Comparison between experimental and calculated results of rising velocity

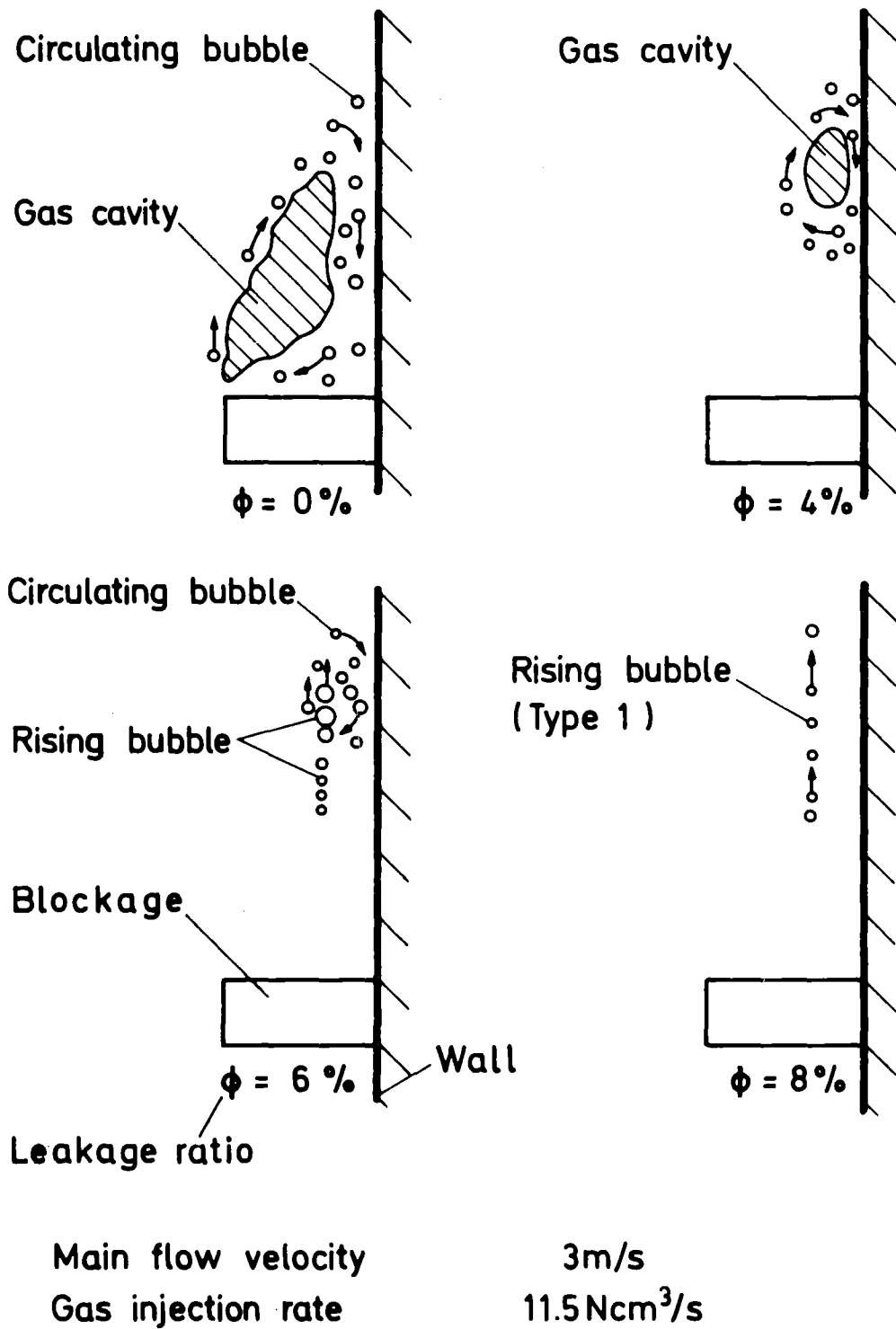
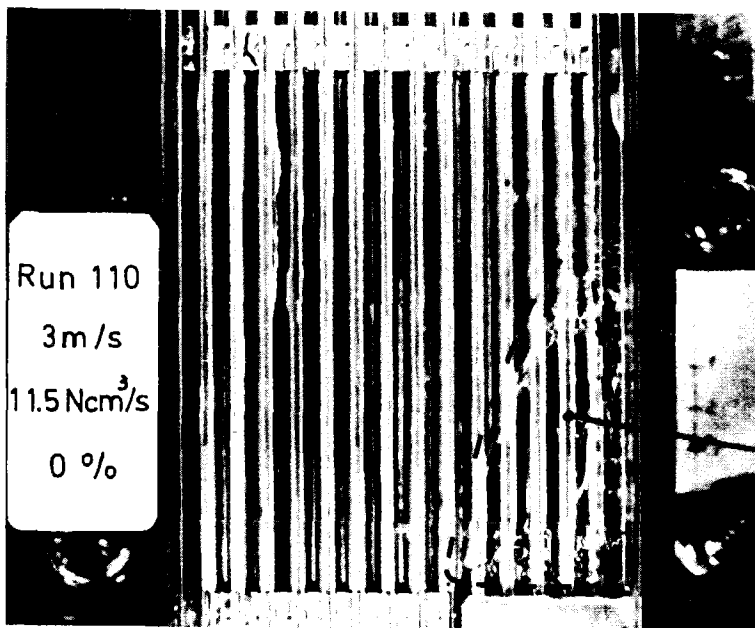


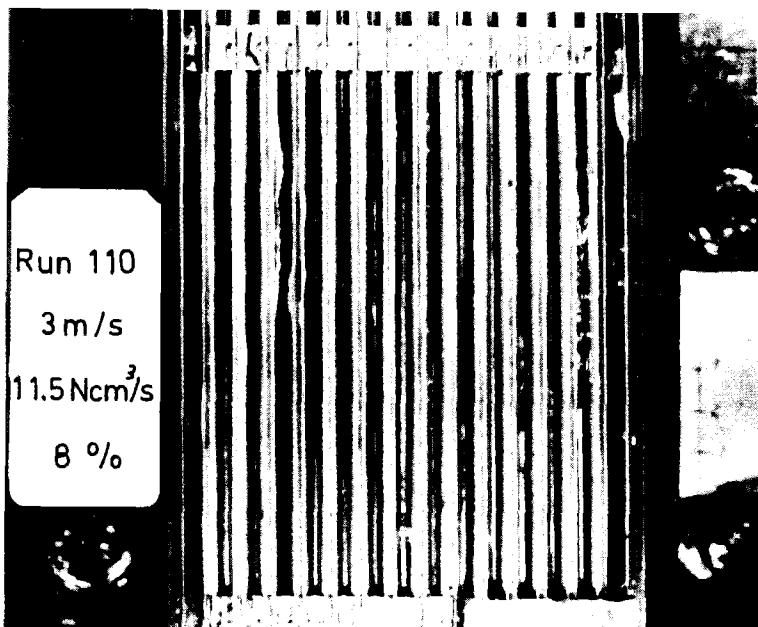
Fig.13 Change of the flow pattern Type 2 to Type 1 with increase of the leakage flow



Run 110
3 m/s
11.5 Ncm³/s
0 %

Leakage ratio
0 %

Gas cavity



Run 110
3 m/s
11.5 Ncm³/s
8 %

Leakage ratio
8 %

Main flow velocity 3 m/s

Gas injection rate 11.5 Ncm³/s



Fig.14 Change of flow pattern from Typ 2 to Typ 1 by increasing leakage flow

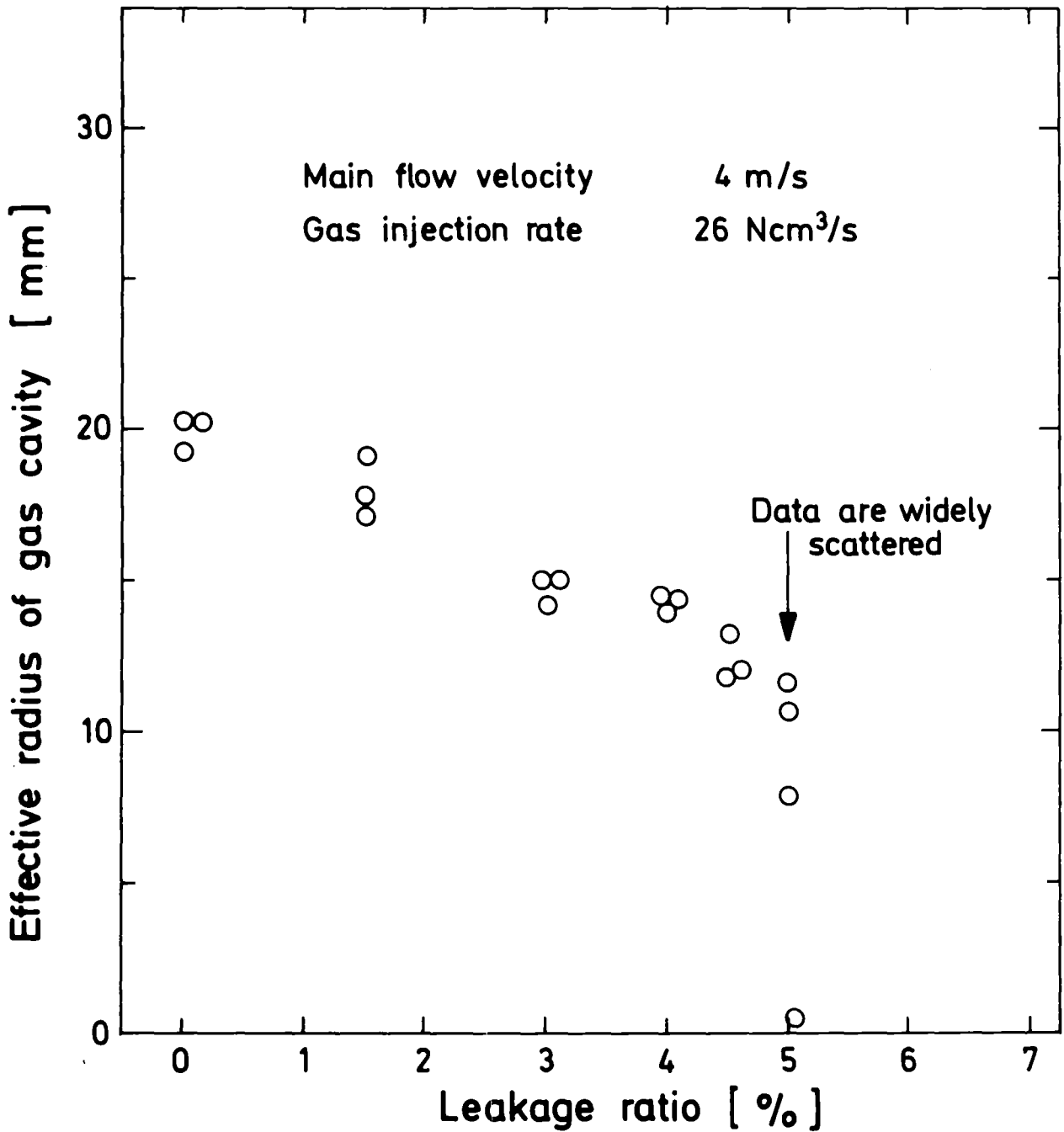


Fig.15 Dependence of gas cavity size on leakage ratio

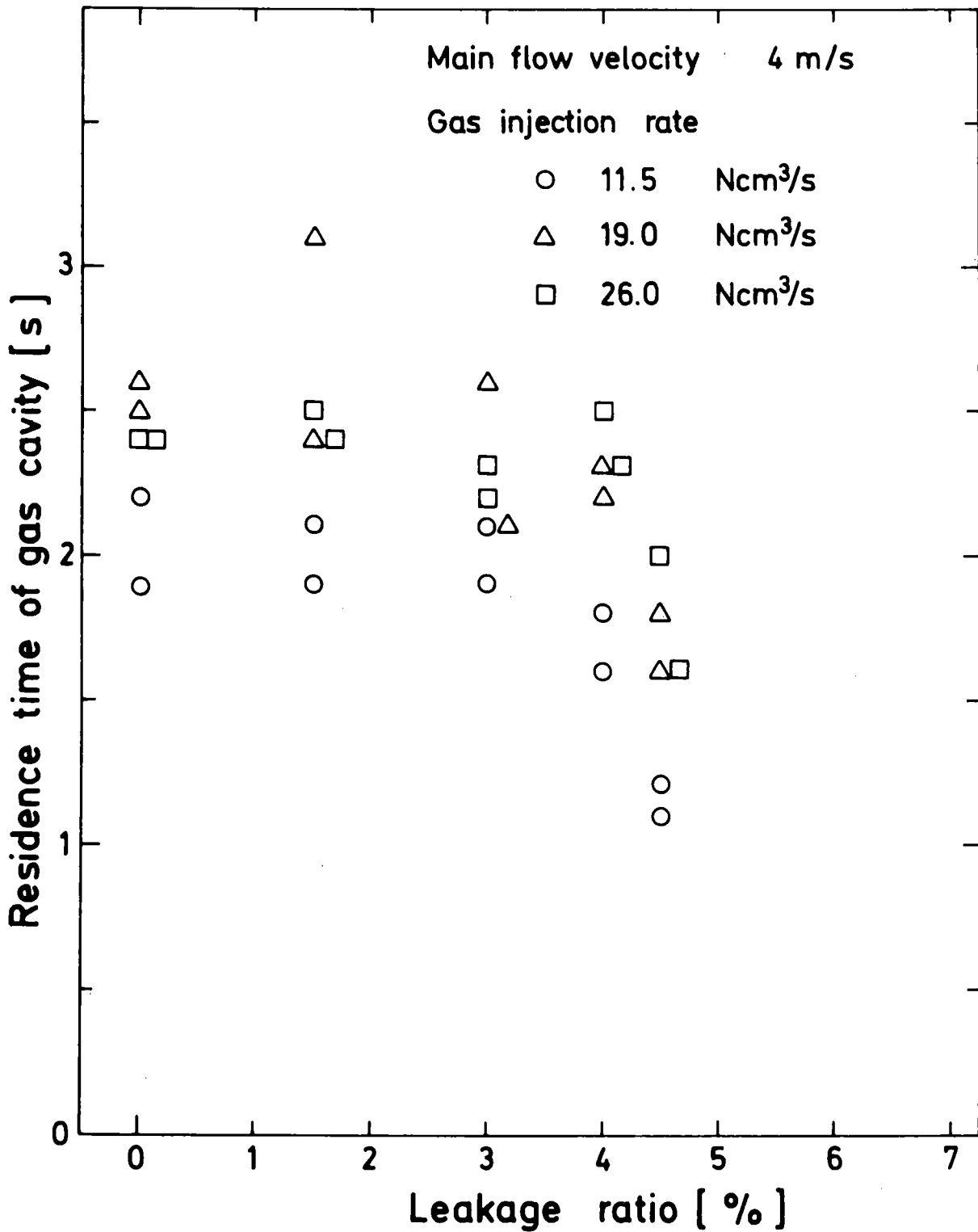
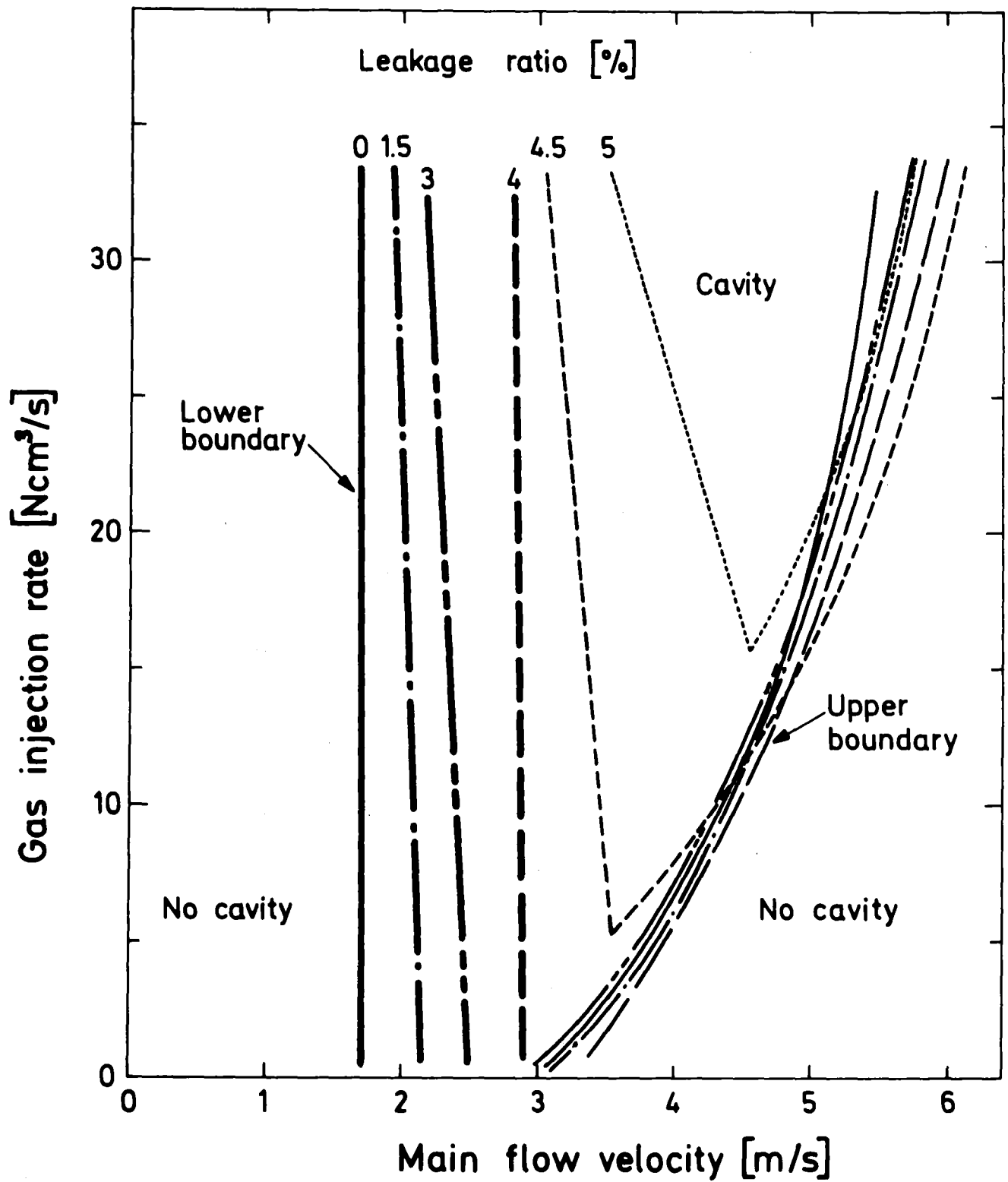


Fig.16 Dependence of the residence time of gas cavity on leakage ratio



KIK

Fig.17 Relation between gas injection rate main flow velocity and flow pattern types for various leakage ratios

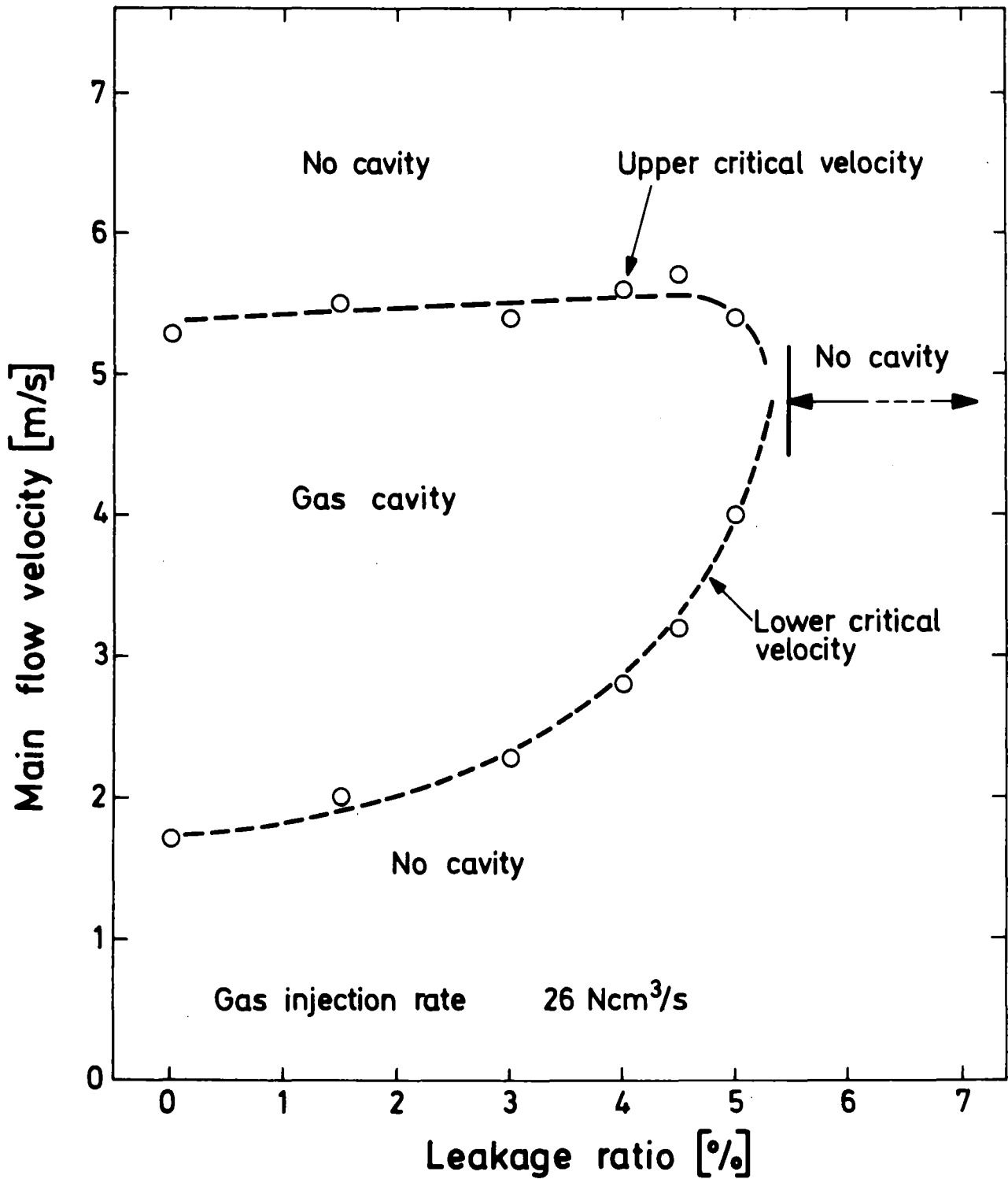
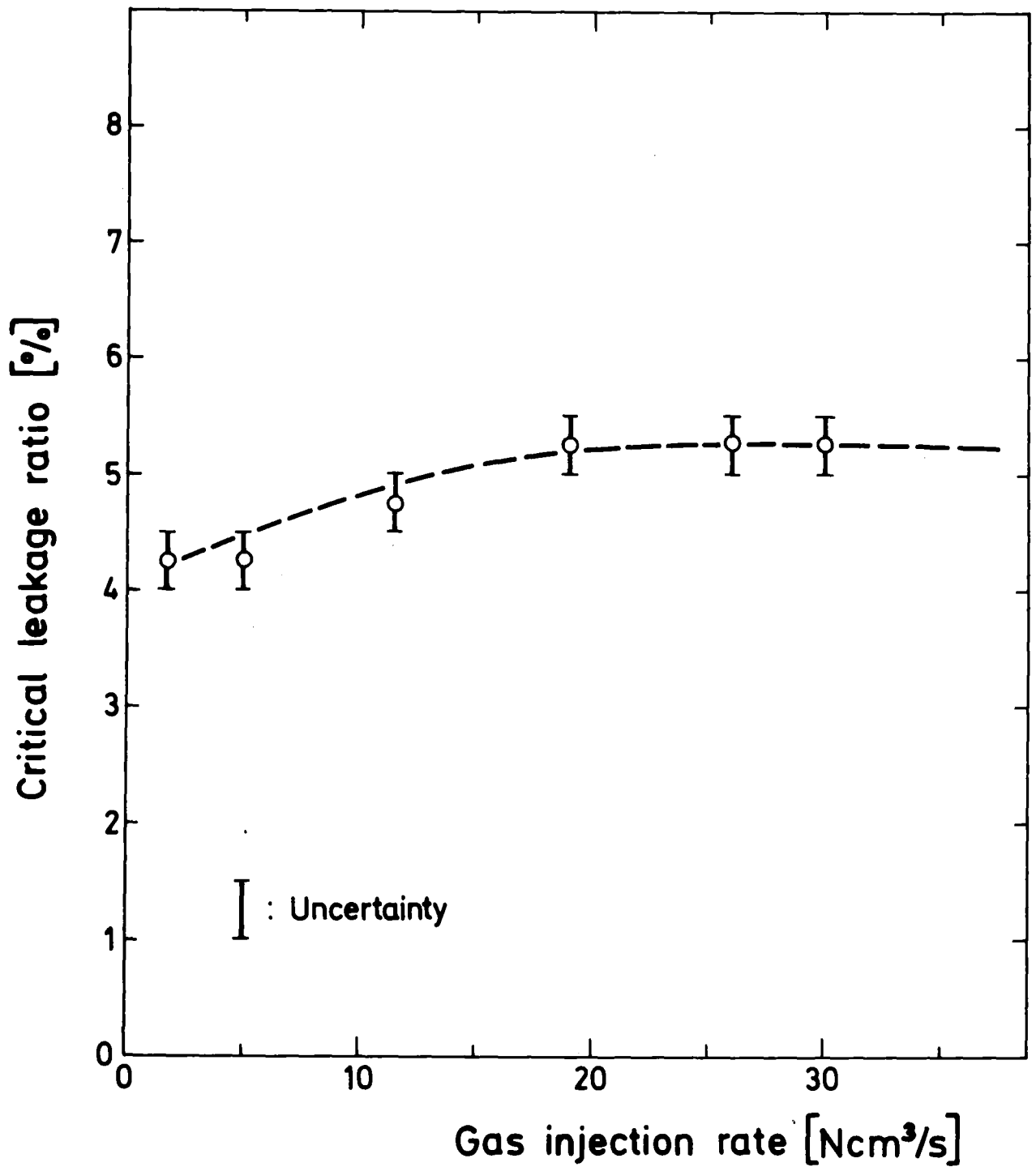
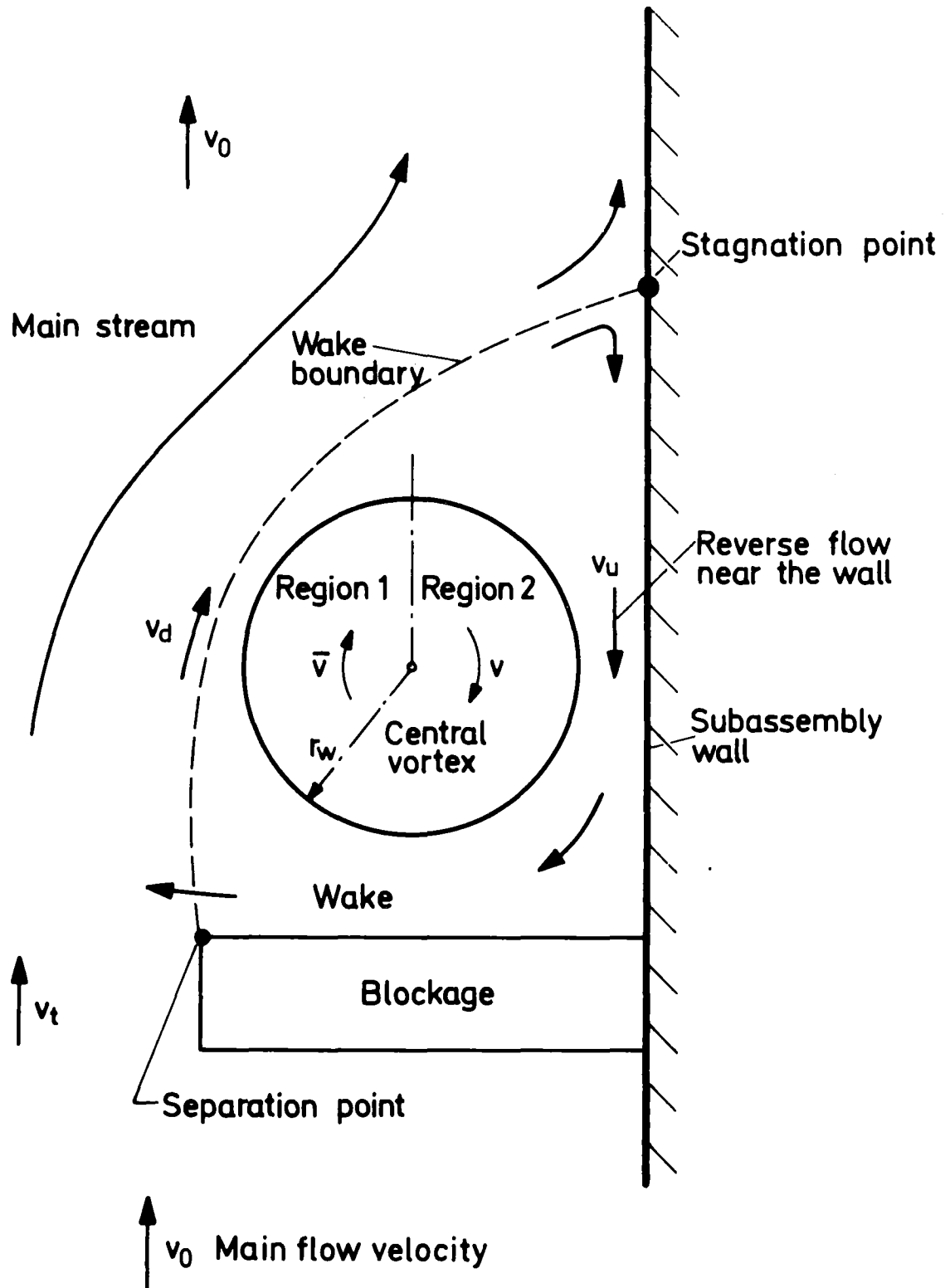


Fig.18 Dependence of critical velocities for gas cavity formation on leakage ratio



KIK

Fig. 19 Dependence of critical leakage ratio for gas cavity dispersion on gas injection rate



KIK

Fig. 20 Model of the flow distribution behind an impermeable blockage [12]

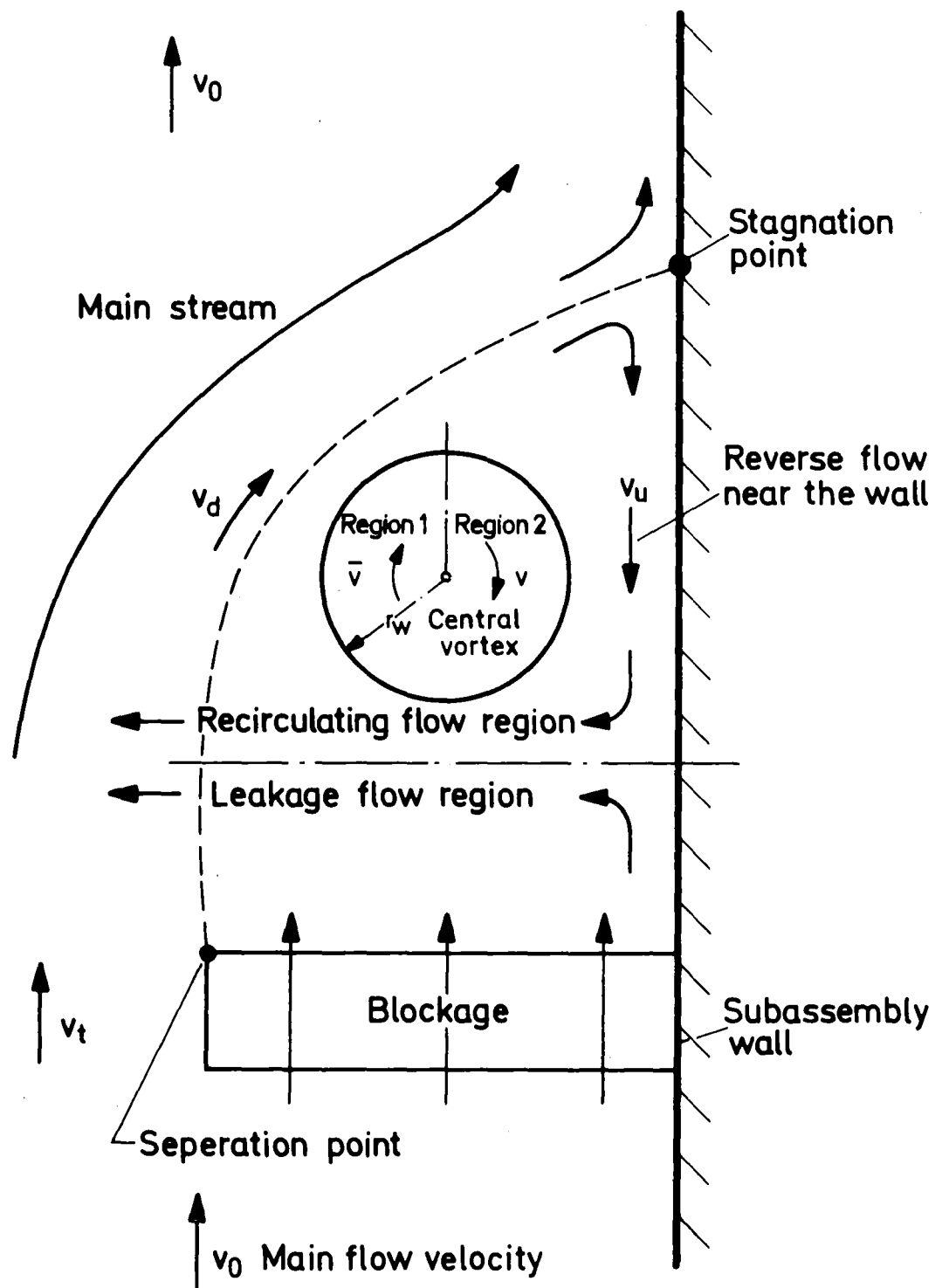
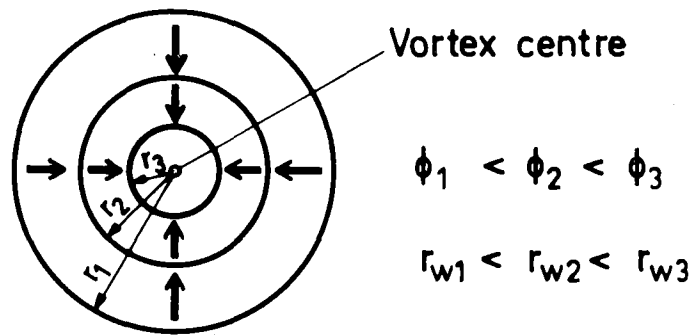
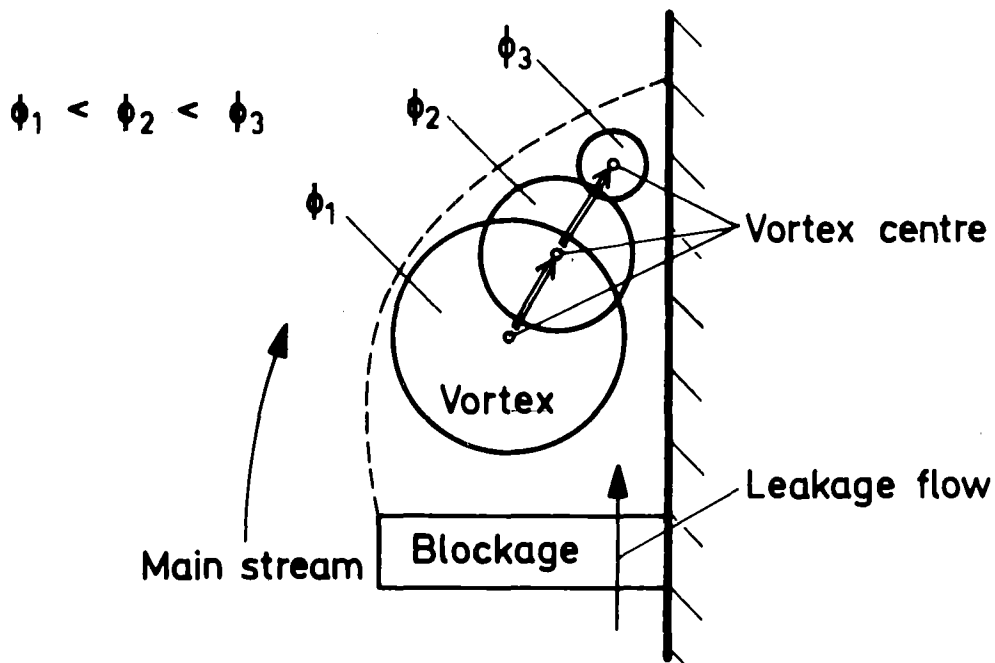


Fig. 21 Model of the flow distribution behind a porous blockage



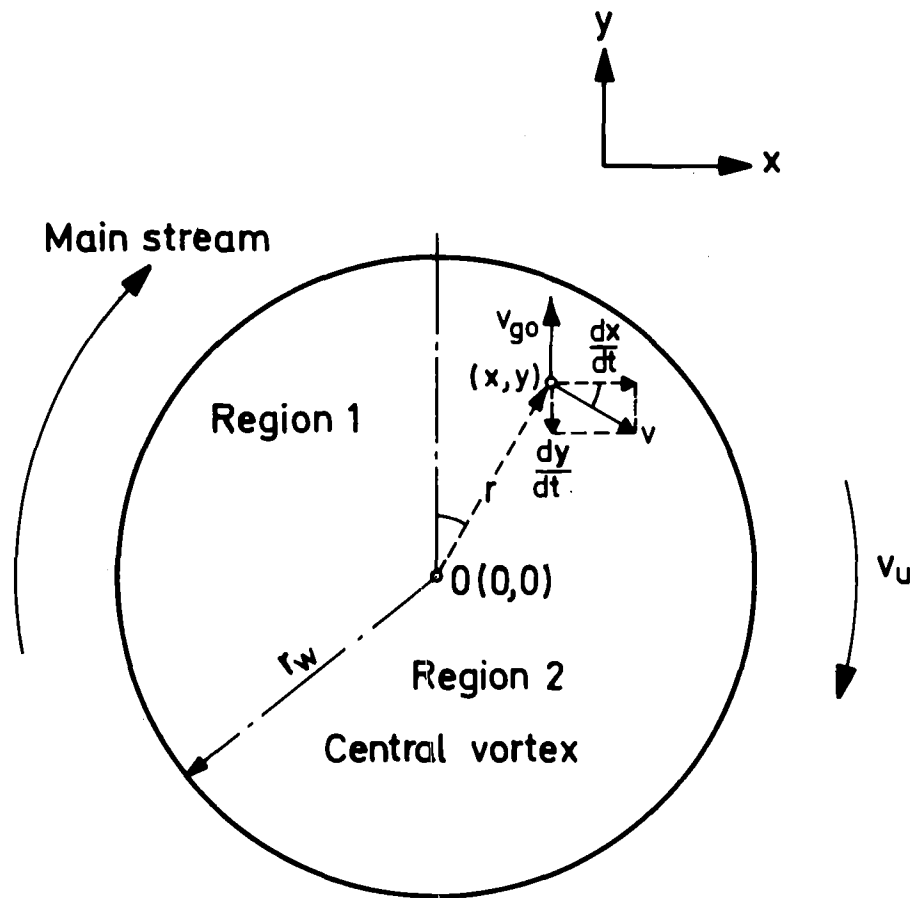
(a) "Fixed - centre" model



(b) "Floating - centre" model

KJK

Fig. 22 Schematic diagram of a comparison between "floating" and "fixed-centre" models



Vortex centre: $(x, y) = (0, 0)$, fixed

Vortex radius: $r_w = f(\phi)$
decreasing with increasing ϕ

KJK

Fig. 23 A fixed-centre model for calculations of bubble motion in the central vortex

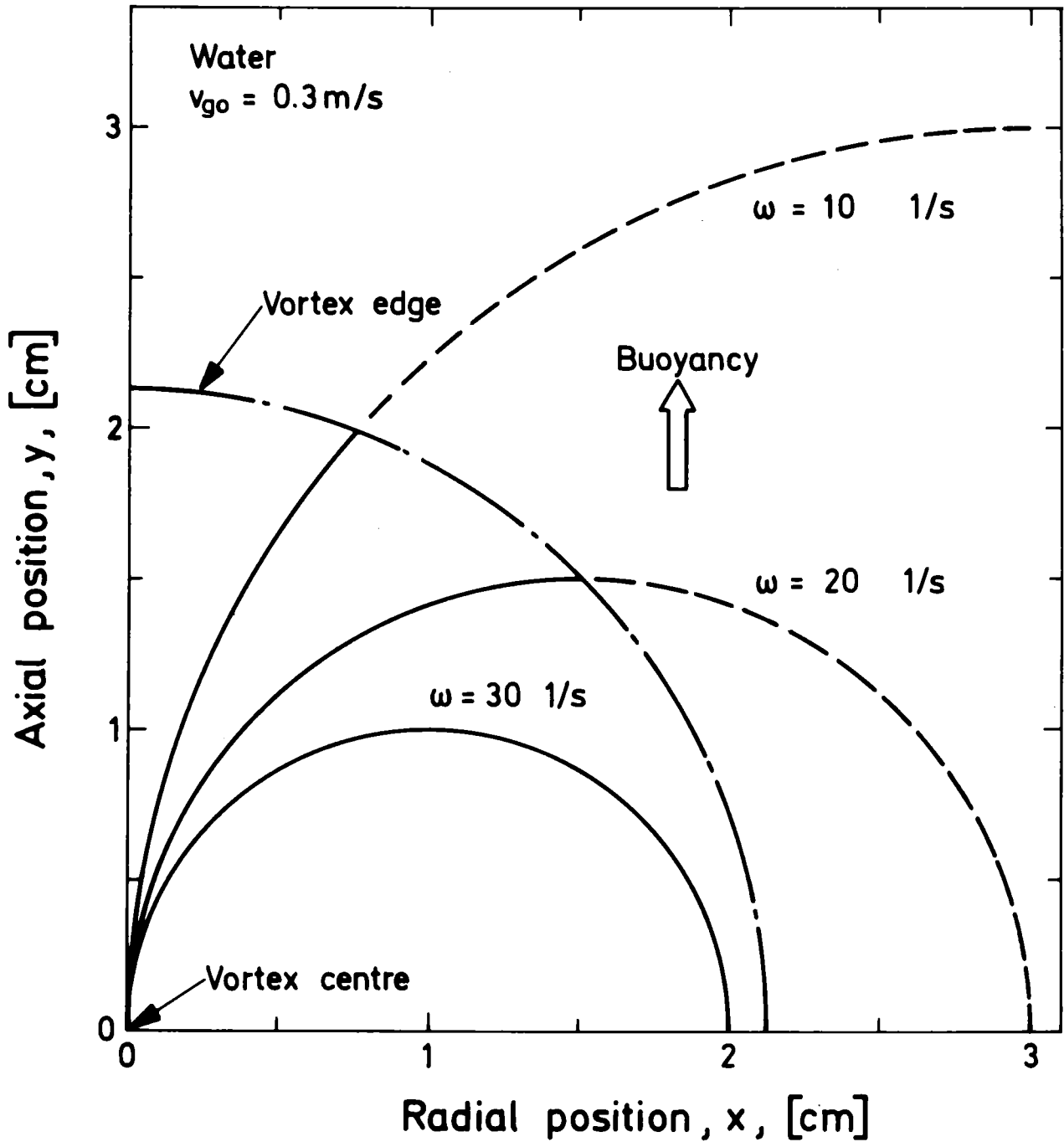


Fig.24 Calculated bubble motion due to buoyancy in Region 2 of the central vortex

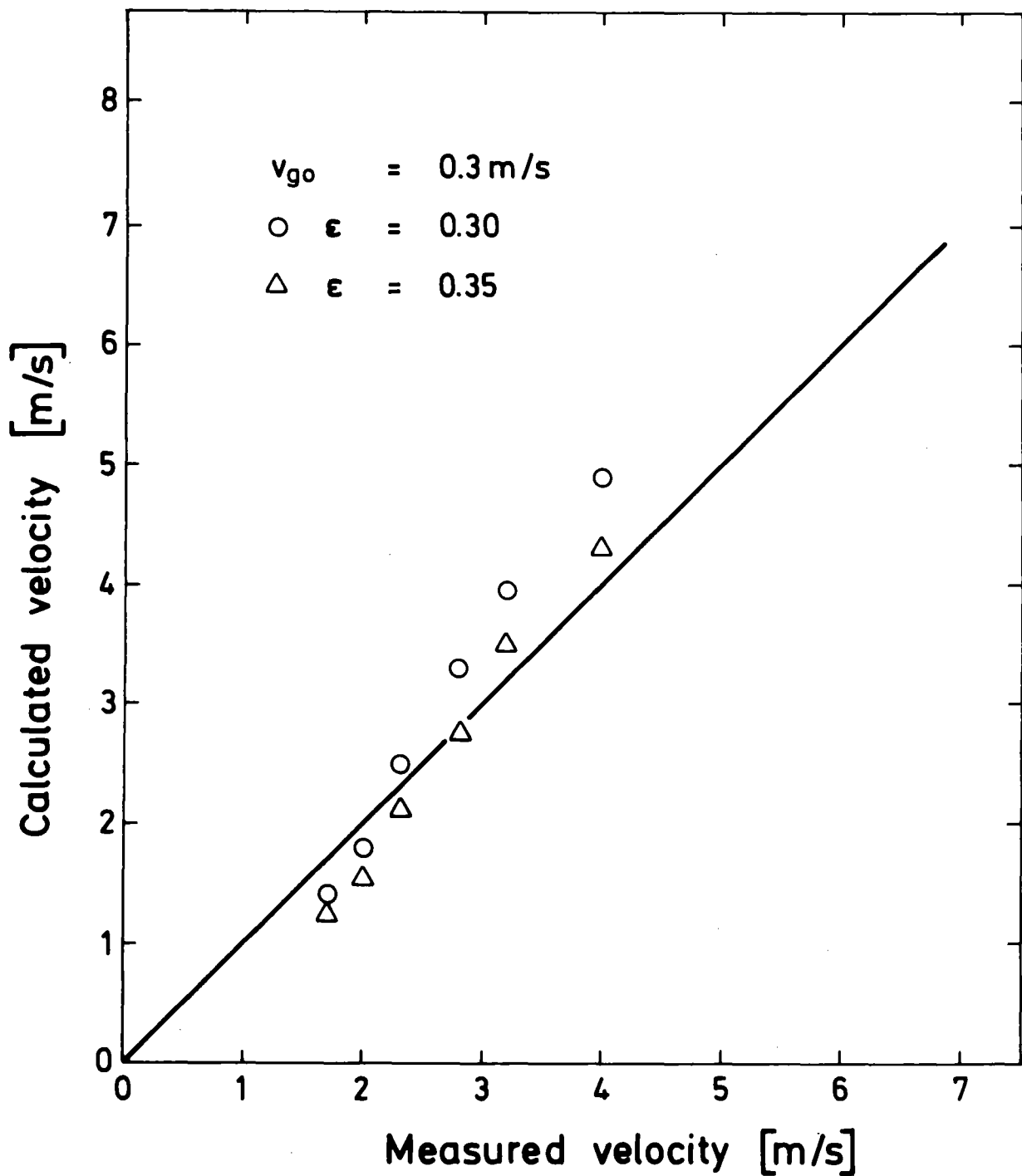


Fig. 25 Comparison between measured and calculated critical velocity of the lower boundary

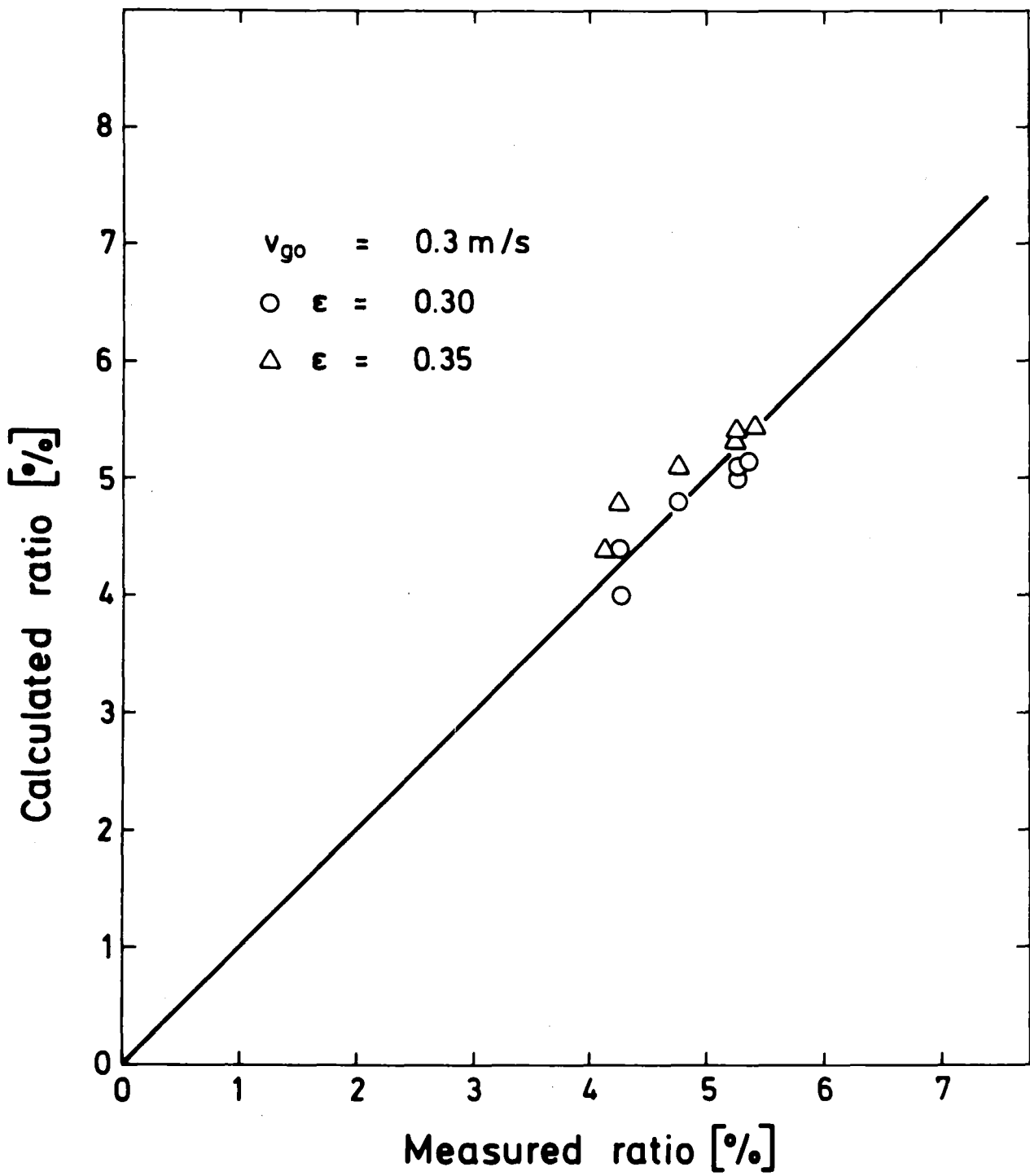


Fig. 26 Comparison between measured and calculated values of critical leakage ratio for gas cavity dispersion

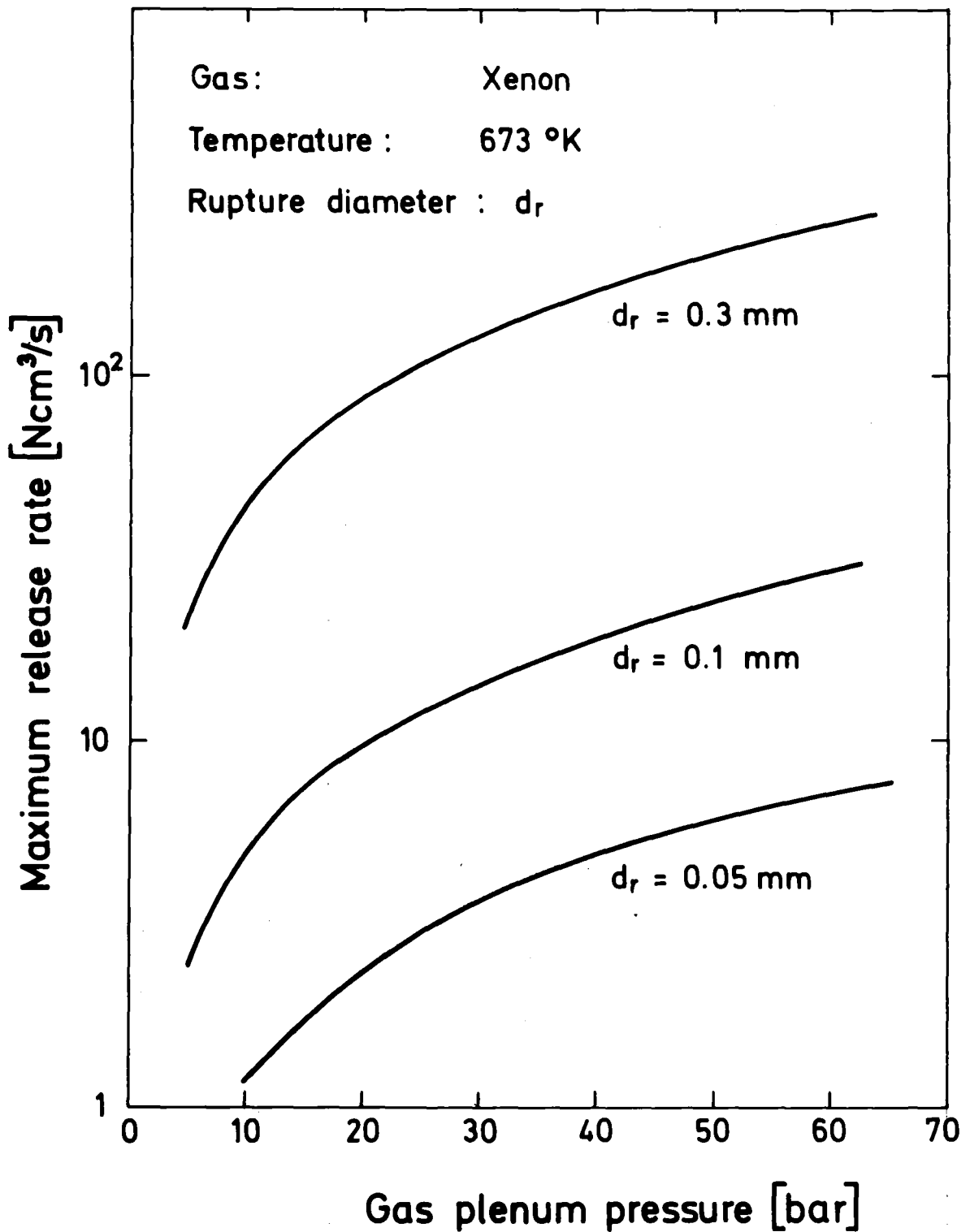


Fig. 27 Maximum gas release rate from a fuel pin

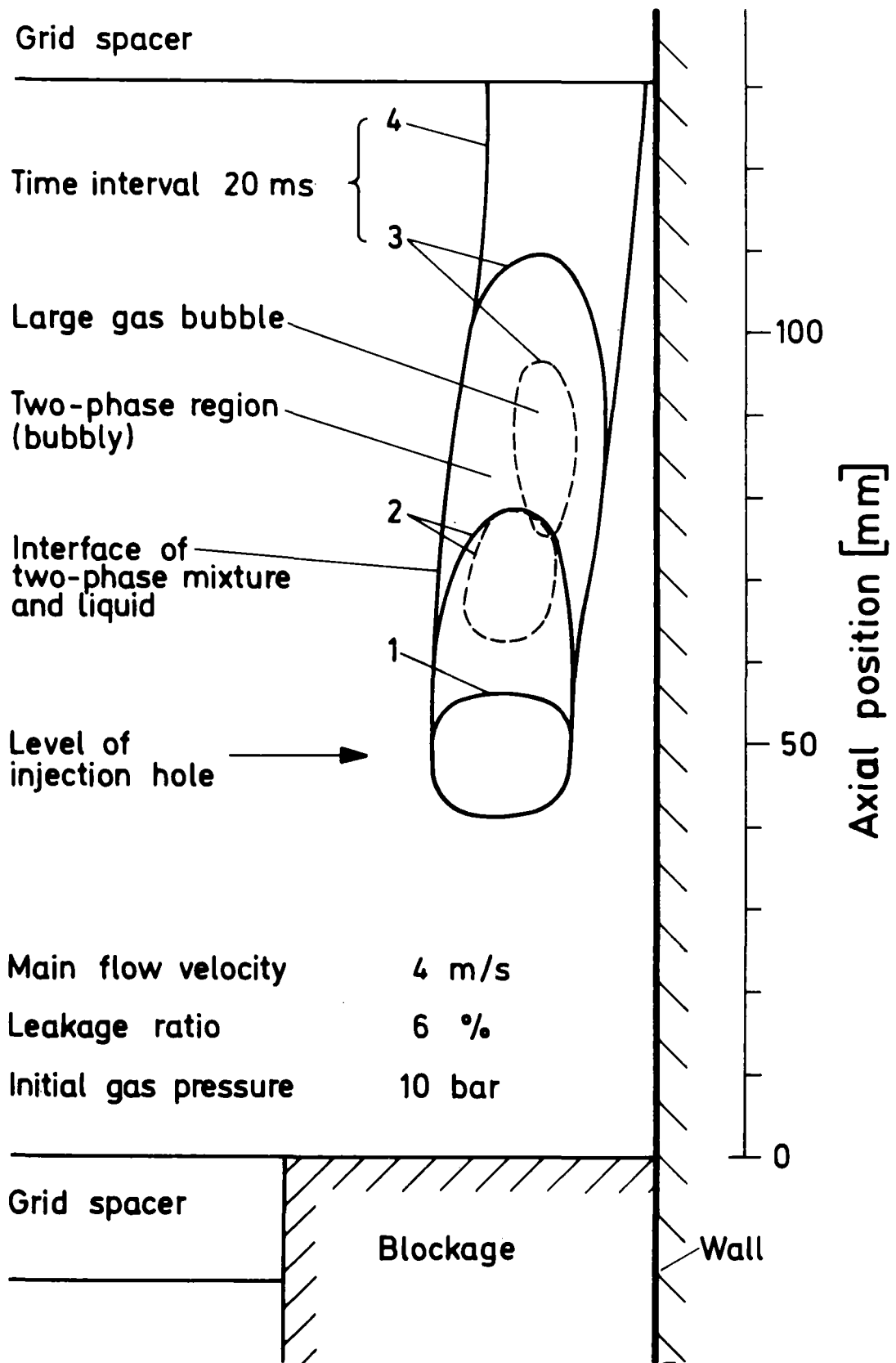


Fig. 28 Transient gas behaviour behind the blockage with leakage flow just after start of gas injection